

# Unidentified sources in the Fermi-LAT second source catalog: the case for DM subhalos

Hannes-S. Zechlin, Dieter Horns

University of Hamburg, Institut für Experimentalphysik,  
Luruper Chaussee 149, D-22761 Hamburg, Germany

E-mail: [hzechlin@physik.uni-hamburg.de](mailto:hzechlin@physik.uni-hamburg.de), [dieter.horns@physik.uni-hamburg.de](mailto:dieter.horns@physik.uni-hamburg.de)

**Abstract.** The Large Area Telescope (LAT) aboard the *Fermi* satellite allows us to study the high-energy  $\gamma$ -ray sky with unprecedented sensitivity. However, the origin of 31% of the detected  $\gamma$ -ray sources remains unknown. This population of unassociated  $\gamma$ -ray sources may contain new object classes, among them sources of photons from self-annihilating or decaying non-baryonic dark matter. *Fermi*-LAT might be capable to detect up to a few of these dark matter subhalos as faint and moderately extended  $\gamma$ -ray sources with a temporally steady high-energy emission. After applying corresponding selection cuts to the second year *Fermi* catalog 2FGL, we investigate 13 candidate objects in more detail including their multi-wavelength properties in the radio, infrared, optical, UV, and X-ray bands. For the  $\gamma$ -ray band, we analyze both the 24-month and 42-month *Fermi*-LAT data sets. We probe the  $\gamma$ -ray spectra for indications of a spectral cutoff, which singles out four sources of particular interest. We find all sources to be compatible with a point-source scenario. Multi-wavelength associations and, in particular, their infrared color-color data indicate no source to be compatible with a dark matter origin, and we find the majority of the candidates to probably originate from faint, high-frequency peaked BL Lac type objects. We discuss possibilities to further investigate source candidates and future prospects to search for dark matter subhalos.

**Keywords:** dark matter experiments, gamma ray experiments, active galactic nuclei

**ArXiv ePrint:** [1210.3852](https://arxiv.org/abs/1210.3852)

---

## Contents

<b>1</b>	<b>Introduction</b>	<b>1</b>
<b>2</b>	<b>Gamma-ray emission of DM subhalos</b>	<b>2</b>
<b>3</b>	<b>DM subhalo candidates in the 2FGL</b>	<b>3</b>
3.1	Source selection	3
3.2	<i>Fermi</i> -LAT data	4
3.3	Spectral analysis	5
3.4	Variability and angular extent	6
3.5	Multi-wavelength counterparts	10
3.5.1	Catalog data	10
3.5.2	WISE data	10
3.5.3	<i>Swift</i> -UVOT/XRT data	11
3.6	Discussion of preselected candidates	12
<b>4</b>	<b>Discussion and conclusions</b>	<b>15</b>
<b>A</b>	<b>Probability distribution of <math>TS_{\text{exp}}</math></b>	<b>17</b>
<b>B</b>	<b>Multi-wavelength association</b>	<b>20</b>

---

## 1 Introduction

Current all-sky surveys of the high-energy (HE)  $\gamma$ -ray sky provide unprecedented sensitivity to disseminate the population of high-energy  $\gamma$ -ray emitters. Based upon 24 months of data recorded with the Large Area Telescope (LAT) aboard the *Fermi Gamma-ray Space Telescope* satellite (*Fermi*) [1], the *Fermi* Collaboration recently published the second *Fermi*-LAT point-source catalog (2FGL) [2]. The 2FGL contains 1 873 sources detected between 100 MeV and 100 GeV (with a significance  $S \gtrsim 4\sigma$ ), whereof approximately one third (576 sources) are lacking reliable association with sources detected in other wavelength bands. On the contrary, the majority ( $\sim 1000$ ) of the 1 297 associated sources have been classified to most likely originate from active galactic nuclei (AGN), in particular BL Lacs and flat spectrum radio quasars [3].

While it seems plausible that most of the unassociated (high-latitude)  $\gamma$ -ray sources are expected to originate from faint AGN, this sample may also contain new classes of  $\gamma$ -ray emitting sources [4–9]. In particular, this includes sources potentially driven by self-annihilating (or decaying) dark matter (DM), i.e., DM subhalos (see [10] and references therein). In this context, it is also interesting to note that the intensity of the isotropic diffuse  $\gamma$ -ray background [11] cannot be fully accounted for by the properties of known  $\gamma$ -ray emitters (e.g., blazars) extrapolated below the confusion limit of *Fermi*-LAT [12, 13]. Unravelling the nature of *Fermi* unidentified sources therefore remains a crucial task to tackle searches and constraints on new HE phenomena, e.g., self-annihilating DM.

Significant evidence for the existence of a so far undiscovered form of matter, so-called DM, has been provided by various different astrophysical observations via its gravitational

imprint [14–16]. Cold DM manifests itself on both cosmological and galactic scales, i.e., prevailing the formation of large scale structures down to accounting for galactic halos and their DM substructure (DM subhalos) [17, 18]. Observations indicate DM as an unknown non-baryonic type of heavy, electrically neutral, and color-neutral particle, which is very weakly interacting with standard model particles. A promising scenario comprises DM to be constituted by weakly interacting massive particles (WIMPs) of Majorana type, with a mass between a few hundred GeV and several TeV. With an interaction strength at the order of weak interactions, thermal production of WIMPs in the early Universe can consistently explain the measured DM relic density [19]. Appropriate WIMP candidates naturally arise in beyond standard model theories, e.g., Supersymmetry [20].

The discovery of WIMPs is then possible via three complementary approaches, i.e., collider, direct, and indirect detection techniques: while WIMPs may be directly produced in colliders with sufficient center-of-mass energy, e.g., the Large Hadron Collider (LHC) [21, 22], underground low-noise experiments [23] are sensitive to their scattering signatures with heavy nuclei. From the astrophysical point of view, WIMPs may be indirectly detected through their self-annihilation (or decay) to standard model final states, eventually producing  $\gamma$  rays, charged light hadrons and leptons, and neutrinos [24].

In this paper, we present a search for DM subhalo candidates in the 2FGL catalog, following up on the 1FGL catalog search we conducted in [10], henceforth called Paper I; for related studies, see e.g. [8, 25–29]. The paper is structured as follows: In section 2, the  $\gamma$ -ray properties of detectable DM subhalos are summarized. The catalog search for candidate  $\gamma$ -ray sources and a study of their spectral and temporal properties are described in section 3, including the investigation of multi-wavelength counterparts and an analysis of archival UV and X-ray data. The results of this study are summarized and discussed in section 4.

## 2 Gamma-ray emission of DM subhalos

In the hierarchical formation of structures, galactic DM halos are anticipated to host a large population of smaller subhalos (up to  $10^{16}$ ). Their mass spectrum  $dN/dM$  follows a power-law distribution over the mass range  $M$  between  $10^{-11}$ – $10^{-3} M_\odot$  and  $\sim 10^{10} M_\odot$ :  $dN/dM \propto M^{-\alpha}$ , where  $\alpha \in [1.9; 2.0]$ , see [17, 18, 30]. While some of the massive subhalos are expected to host the Milky Way’s luminous dwarf spheroidal satellite galaxies (dSphs), baryonic content of low-mass subhalos and even concentrated massive subhalos can be lacking, see [31, 32] and references therein. In Paper I, we have shown that *up to two* massive DM subhalos between  $10^5$  and  $10^8 M_\odot$  could be detectable with *Fermi*-LAT within the first two mission years, assuming common models on the self-annihilation of heavy WIMPs, their density distribution in DM subhalos, and the distribution of the subhalos in the Galaxy. These objects at distances of  $\mathcal{O}(\text{kpc})$  would appear in the  $\gamma$ -ray sky as moderately extended ( $\theta_{68} \approx 0.5^\circ$ )  $\gamma$ -ray sources above 10 GeV.<sup>1</sup> The faint, temporally constant  $\gamma$ -ray flux at energies  $E$  between 10 and 100 GeV is anticipated at the detection level of *Fermi*-LAT,  $\phi_p(10\text{--}100 \text{ GeV}) \approx 10^{-10} \text{ cm}^{-2} \text{ s}^{-1}$ , owing to the small self-annihilation cross section of WIMPs,  $\langle\sigma v\rangle \sim 3 \times 10^{-26} \text{ cm}^3 \text{ s}^{-1}$ . The differential  $\gamma$ -ray flux approximately follows a hard power-law (index  $\Gamma \lesssim 1.5$ ) with a distinct cutoff to the WIMP mass  $m_\chi$ , where we assumed WIMPs of  $m_\chi = 500$  (150) GeV annihilating to heavy quarks, gauge bosons (e.g.,  $b\bar{b}$ ,  $W^+W^-$ ), or

<sup>1</sup>Within the angle  $\theta_{68}$  a fraction of 68% of the total  $\gamma$ -ray luminosity is emitted. In comparison with the point spread function of *Fermi*-LAT,  $\theta_{68} = 0.5^\circ$  corresponds to about  $4\sigma_{\text{PSF}}$ , where  $\sigma_{\text{PSF}} \approx 0.13^\circ$  at 10 GeV (see [http://www.slac.stanford.edu/exp/glast/groups/canda/lat\\_Performance.htm](http://www.slac.stanford.edu/exp/glast/groups/canda/lat_Performance.htm)).

to the leptons  $\tau^+\tau^-$ , see figure 2 in Paper I. We emphasize that the expected  $\gamma$ -ray flux may be even higher when including the possible presence of sub-substructures (enhancement by a factor of 2 to 3) [33, 34] and (rather model-dependent) photon contributions from final state radiation and virtual internal Bremsstrahlung [35–38]. The rather low WIMP velocity in bound subhalos might also lead to resonances in the self-annihilation cross section (Sommerfeld enhancement) [39, 40]. Potential secondary emission from energetic charged leptons eventually produced by WIMP annihilation in Galactic photon and magnetic fields is expected to be rather faint and diffuse, e.g. [41–43], and we therefore anticipate DM subhalos to be  $\gamma$ -ray sources which are not associated to sources detected in other wavelength bands at lower energies.

### 3 DM subhalo candidates in the 2FGL

#### 3.1 Source selection

The selection of candidate objects in the class of unidentified sources listed in the 2FGL<sup>2</sup> is based upon the properties of  $\gamma$ -ray emitting DM subhalos discussed above:

- (i) The sample was reduced to sources at high galactic latitudes  $|b| \geq 20^\circ$ , to avoid confusion with conventional Galactic sources and to reduce the impact of diffuse Galactic  $\gamma$ -ray emission.
- (ii) Sources were selected for a steady  $\gamma$ -ray flux, requiring the cataloged variability parameter  $var < 41.64$ , which corresponds to a probability of  $P_s > 1\%$  for the source to be steady.
- (iii) To select sources potentially driven by massive WIMPs, a detection above 10 GeV was required. In addition, most of the high-energy pulsars located at high Galactic latitude are eliminated by this energy cut. Spectrally,  $\gamma$ -ray pulsars may resemble DM subhalos, given their stable emission of characteristically hard  $\gamma$ -ray spectra ( $\Gamma < 2$ ) with typical cutoff energies  $E_c$  between 1 and 10 GeV [44–47].
- (iv) Spectrally hard sources were selected constraining the index of the cataloged power-law fit with  $\Gamma < 2.0$ .

All but the last cut have been already used in Paper I. Applying cuts (i) to (iv) to the unassociated sources listed in the 2FGL, 14 unassociated  $\gamma$ -ray sources remain. With the exception of 2FGL J2339.6–0532, all other sources have a HE flux close to the detection level of *Fermi*-LAT. This is consistent with the expectation for candidate sources as discussed in section 2. We therefore discarded the outstandingly bright object 2FGL J2339.6–0532. Table 1 lists the final sample of 13 candidate sources together with their positional and spectral properties.

The source 2FGL J0031.0+0724 has been extensively studied in Paper I, where also 2FGL J0143.6–5844 has been listed. An updated discussion of 2FGL J0031.0+0724 is presented below. 2FGL J2257.9–3646 has been claimed as a DM subhalo candidate in [29], while very high-energy ( $E > 100$  GeV) follow-up observations of 2FGL J2347.2+0707 have been conducted with MAGIC [27]. All remaining sources are new candidates.

---

<sup>2</sup>Version *v06*

2FGL name	$l, b$ [deg]	$\sigma_{68}/\sigma_{95}$ [arcmin]	$S$ [ $\sigma$ ]	$\Gamma$	$\phi_p(10-100 \text{ GeV})$ [ $10^{-10} \text{ cm}^{-2} \text{ s}^{-1}$ ]	$S_5$ [ $\sigma$ ]
J0031.0+0724 <sup>1st</sup>	114.095, -55.108	4.4/7.2	4.4	$1.9 \pm 0.3$	$0.7 \pm 0.3$	4.5
J0116.6-6153	297.749, -54.986	3.7/6.0	5.5	$1.6 \pm 0.2$	$0.7 \pm 0.3$	4.9
J0143.6-5844 <sup>1st</sup>	290.468, -57.102	2.4/3.8	14.2	$1.7 \pm 0.1$	$2.2 \pm 0.6$	9.5
J0305.0-1602 <sup>1st</sup>	200.151, -57.146	4.5/7.3	5.3	$1.5 \pm 0.2$	$0.9 \pm 0.4$	4.4
J0312.8+2013	162.507, -31.569	3.7/6.0	4.4	$1.7 \pm 0.2$	$0.7 \pm 0.3$	4.5
J0338.2+1306	173.471, -32.929	3.9/6.3	5.8	$1.5 \pm 0.2$	$1.1 \pm 0.5$	5.1
J0438.0-7331	286.088, -35.168	4.1/6.6	6.1	$1.4 \pm 0.2$	$0.8 \pm 0.4$	5.0
J0737.5-8246	295.086, -25.467	3.7/6.0	4.4	$1.3 \pm 0.3$	$1.0 \pm 0.4$	5.2
J1223.3+7954	124.470, +37.134	3.6/5.8	4.2	$1.4 \pm 0.3$	$0.6 \pm 0.3$	4.6
J1347.0-2956	317.047, +31.398	4.1/6.6	5.0	$1.4 \pm 0.3$	$1.0 \pm 0.5$	4.2
J1410.4+7411	115.839, +41.825	2.9/4.7	9.1	$1.9 \pm 0.1$	$0.7 \pm 0.3$	4.7
J2257.9-3646 <sup>1st</sup>	3.899, -64.186	5.0/8.2	5.3	$1.9 \pm 0.2$	$0.8 \pm 0.4$	4.1
J2347.2+0707 <sup>1st</sup>	96.214, -52.385	3.7/5.9	7.2	$2.0 \pm 0.2$	$0.8 \pm 0.4$	4.1

**Table 1:** DM subhalo candidates in the 2FGL catalog. The first column lists the 2FGL name, where the index “1st” flags sources which have already been listed in the 1FGL (i.e., 1FGL J0030.7+0724, 1FGL J0143.9-5845, 1FGL J0305.2-1601, 1FGL J2257.9-3643, and 1FGL J2347.3+0710). For each source, the position is given in galactic coordinates ( $l, b$ ), together with the positional uncertainty  $\sigma_{68(95)}$  [68% (95%) c.l., semi-major axis], detection significance  $S$  in Gaussian sigma, the power-law index  $\Gamma$ , and the photon flux in the 10–100 GeV band. The last column  $S_5$  lists the significance of the 10–100 GeV detection (in Gaussian sigma).

### 3.2 *Fermi*-LAT data

The data analysis of each object in table 1 was based on data recorded with the *Fermi*-LAT in the first 24 as well as 42 months<sup>3</sup> of the mission.<sup>4</sup> We chose the same analysis framework and recommended options that were used for the 2FGL (based upon 24 months of data), with the exception that the considered energy range was extended to cover 100 MeV to 300 GeV. The data analysis was performed with the public version of the Fermi Science Tools (v9r23p1, release date 06 October 2011) using data of Pass-7 event reconstruction along with the P7\_V6 instrument response functions.<sup>5</sup> All events passing the SOURCE event class were considered. Events were filtered for a maximum zenith angle of  $100^\circ$  (to eliminate contamination from the Earth’s limb), a maximum rocking-angle of  $52^\circ$ , and the recommended quality filters DATA\_QUAL == 1 and LAT\_CONFIG == 1 were applied. The (quadratic) region-of-interest (RoI) was centered on the nominal 2FGL position of the source-of-interest (SoI) with a size of  $20^\circ \times 20^\circ$ . The overall spectral fit was performed using the binned likelihood method (with 10 energy-bins per decade; optimizer NEWMINUIT, requiring an absolute fit tolerance of  $10^{-3}$ ), where the source model contained all 2FGL sources within the RoI, along with fixed cataloged positional and spectral parameters. Including the SoI, the normalizations  $\phi_0$  and indices  $\Gamma$  of the default model of a power-law spectrum [ $d\phi/dE = \phi_0 (E/E_0)^{-\Gamma}$ ]

<sup>3</sup>The 42-month data set covers the time period between the beginning of August 2008 (239557419 MET) up to the beginning of February 2012 (350063020 MET).

<sup>4</sup>The LAT data are publicly available at <http://fermi.gsfc.nasa.gov/ssc/data/>.

<sup>5</sup>See <http://fermi.gsfc.nasa.gov/ssc/data/analysis/>.

of the innermost six sources were kept free, while the energy scale  $E_0$  was fixed to the cataloged pivot energy. We used the latest publicly available models for the Galactic foreground (*gal\_2yearp7v6\_v0.fits*) and isotropic background emission (*iso\_p7v6source.txt*). The normalization and corrective power-law index of the Galactic foreground template and the normalization of the isotropic background template were left free. In detail, the analysis was performed with the tools *gtselect*, *gtmktime*, *gtbin*, *gtltcube*, *gtexpcube2*, *gtsrcmaps*, and *gtlike*. For each source, we checked that our overall fit reproduced the cataloged data sufficiently.

The analysis chain for the 42-month data set allowed for a possible change of the positional coordinates of each SoI. We used *gtfindsrc* to refit the position. The refined uncertainty contour (at 95% confidence level) was computed from the two-dimensional likelihood function  $\mathcal{L}(\text{RA}, \text{Dec})$ , requiring  $2\Delta(\log \mathcal{L}) = 6.18$  (2 degrees of freedom).

### 3.3 Spectral analysis

The energy spectra of the candidate sources have to be consistent with a spectrum generated by self-annihilating WIMPs. For each candidate source, we carried out a statistical hypotheses test based upon a likelihood ratio. The null hypothesis ( $H_{\text{pl}}$ ) of the SoI to follow a conventional power-law spectrum was tested against the hypothesis ( $H_{\text{exp}}$ ) of a spectrum generated by WIMP annihilation. The likelihood ratio defines the test statistic

$$\text{TS}_{\text{exp}} = -2 \ln \left( \frac{\mathcal{L}(H_{\text{pl}})}{\mathcal{L}(H_{\text{exp}})} \right), \quad (3.1)$$

where  $\mathcal{L}(H)$  denotes the total likelihood for the corresponding RoI, fitted assuming the SoI to follow the spectral hypothesis  $H$  (cf. section 3.2).<sup>6</sup>

As benchmark models, we probed for WIMP annihilation to heavy quarks (e.g.,  $b\bar{b}$ ), gauge bosons (e.g.,  $W^+W^-$ ), and to the leptons  $\tau^+\tau^-$ , which lead to a considerably harder  $\gamma$ -ray spectrum. For our purpose, the differential  $\gamma$ -ray spectra resulting from annihilation of supersymmetric neutralinos to the afore mentioned final states, see [48, 49], can be approximated with a power-law spectrum modified by an exponential cutoff [50],  $dN_\gamma/dx = N_0 x^{-\Gamma} \exp(-px)$ , where  $x = E/m_\chi$ . This simple parametrization originally introduced for gauge boson final states [50] also provides a reasonable fit to the  $\tau^+\tau^-$  final states [49] with different values of  $N_0$ ,  $\Gamma$ , and  $p$ . The used parameters are listed in table 2. This approach simplifies considerably the treatment and interpretation of the fit procedure. Given the small number statistics of the faint sources, more subtle differences in the final state spectrum cannot be resolved.

Therefore, the hypothesis  $H_{\text{exp}}$  was a power-law spectrum with exponential cutoff,  $d\phi/dE = \phi_0 (E/E_0)^{-\Gamma} \exp(-E/E_c)$ . The WIMP mass is then connected to the cutoff energy via  $m_\chi = p E_c$ , and the normalization is  $\phi_0 = N_0 m_\chi^{\Gamma-1} E_0^{-\Gamma}$ . The index  $\Gamma$  was fixed to the values given in table 2, while the energy scale was set to  $E_0 = 1 \text{ GeV}$ . As discussed in section 3.1, we note that this hypothesis also probes for  $\gamma$ -ray pulsars which might contaminate our sample, even though we expect most of them to be eliminated by the energy cut.

Since  $\Gamma$  was kept fixed for  $H_{\text{exp}}$ , the null and alternative hypotheses are not nested. This implies that the test statistic  $\text{TS}_{\text{exp}}$  does not necessarily follow the theorems of Wilks [51] or Chernoff [52], i.e.,  $\text{TS}_{\text{exp}}$  is not drawn from a chi-square distribution in the null hypothesis.

---

<sup>6</sup>Note that the spectral models (usually power laws) of all other sources in the RoI are kept fixed. Therefore, another possibility would be to use the test statistic  $\text{TS}$  assigned by the spectral likelihood fit (*gtlike*) to measure the source's detection significance,  $S \propto \sqrt{\text{TS}}$ . We checked that both methods give similar results, as expected.

Channel	$N_0$	$\Gamma$	$p$	Remarks
heavy quarks, gauge bosons	0.73	1.5	7.8	[50]
$\tau^+\tau^-$	5.28	0.35	4.6	

**Table 2:** Fit parameters to approximate the differential photon spectra originating from final-state fragmentation of self-annihilating neutralinos by power laws with exponential cut-offs. For annihilation to heavy quarks and gauge bosons, we use the spectral parametrization from [50], while the photon yield from annihilation in  $\tau^+\tau^-$  is approximated from [49].

It also implies that  $\text{TS}_{\text{exp}}$  can have both negative and positive values: the hypothesis  $H_{\text{exp}}$  is disfavored if  $\text{TS}_{\text{exp}} \ll 0$  and favored if  $\text{TS}_{\text{exp}} \gg 0$ . Since the distribution of the test statistic is a priori not known, the significance of this test had to be calculated with Monte Carlo simulations. The methods are described in appendix A. Based upon the simulations, we find that for the index  $\Gamma = 1.5$  (0.35), a significance of  $2\sigma$  corresponds to  $\text{TS}_{\text{exp}} = -6$  ( $-20$ ) and  $\text{TS}_{\text{exp}} = 2$  (2), respectively, while the  $3\sigma$  contour is given by  $\text{TS}_{\text{exp}} = -25$  ( $-35$ ) and  $\text{TS}_{\text{exp}} = 4$  (7); table 8 lists further significance and their corresponding  $\text{TS}_{\text{exp}}$  values.

The best-fit parameters for a fixed  $\Gamma = 1.5$  and  $\Gamma = 0.35$  are summarized in table 3 for the 24-month data and in table 4 for the 42-month data. Although the fitted spectrum depends on just two free parameters, the statistical errors of the normalization and cutoff energy remain comparably large, owing to the sample of very faint sources studied.<sup>7</sup> For the 24-month data, we find that a power-law with exponential cutoff spectrum is favored for the sources 2FGL J0305.0–1602 and 2FGL J0338.2+1306, with a significance of  $2.4\sigma$  and  $3.3\sigma$ , respectively. After 42 months, for both sources the significance of this initial indication has decreased. However, an exponential cutoff is now favored for the sources 2FGL J0143.6–5844 and 2FGL J1410.4+7411, with significances of  $\sim 3\sigma$ . Vice versa, note that for no source we find such a spectrum to be disfavored by the data (i.e., by more than  $3\sigma$ ).

The initial indications for an exponential cutoff in the 24-month or 42-month data sets motivate a closer inspection of the sources 2FGL J0305.0–1602, 2FGL J0338.2+1306, 2FGL J0143.6–5844, and 2FGL J1410.4+7411. A comprehensive discussion of each source candidate is given in section 3.6.

### 3.4 Variability and angular extent

A  $\gamma$ -ray signal from a DM subhalo is expected to be constant in time and may be resolved as an extended source. Therefore, the temporal and spatial distributions of high-energy photons were tested for compatibility with a constant flux and the hypothesis of angular extent. The method used is based upon our previous work in Paper I. Most of the source candidates have been detected exclusively in the upper energy bins with a comparably low background contamination. Therefore, the tests were applied to the high-energy photon distribution between 3–300 GeV and the inclusive interval 10–300 GeV, respectively. As motivated in section 2 (for details see Paper I), high-energy photons within a circular region of radius  $0.5^\circ$  around the nominal 2FGL position were examined. Due to the low background contamination, this sample is dominated by signal events (see below).

<sup>7</sup>Note that the errors quoted in tables 3 and 4 are correlated, given that the energy scale  $E_0$  was fixed to 1 GeV. Choosing the decorrelation energy, in principle, reduces the statistical errors.

24 months	$\Gamma = 1.5$			$\Gamma = 0.35$		
2FGL name	$\phi_0/10^{-11}$ [(cm <sup>2</sup> s GeV) <sup>-1</sup> ]	$E_c$ [GeV]	TS <sub>exp</sub>	$\phi_0/10^{-11}$ [(cm <sup>2</sup> s GeV) <sup>-1</sup> ]	$E_c$ [GeV]	TS <sub>exp</sub>
J0031.0+0724	17.1 ± 8.0	67 ± 84	-2.2	1.3 ± 1.1	21 ± 12	-5.8
J0116.6-6153	20.0 ± 9.0	34 ± 33	0.9	4.7 ± 4.2	9 ± 5	-0.4
J0143.6-5844	70.5 ± 13.2	46 ± 25	1.4	16.8 ± 5.5	10 ± 2	-17.2
J0305.0-1602	21.1 ± 7.5	70 ± 78	1.4	4.8 ± 2.7	12 ± 5	4.1
J0312.8+2013	29.9 ± 11.7	46 ± 40	-0.6	2.8 ± 2.1	16 ± 8	-5.2
J0338.2+1306	48.0 ± 13.5	40 ± 28	4.2	12.6 ± 5.9	9 ± 3	6.7
J0438.0-7331	24.5 ± 9.4	105 ± 134	0.9	3.8 ± 2.5	17 ± 8	1.1
J0737.5-8246	31.6 ± 11.8	66 ± 68	1.3	5.0 ± 2.8	14 ± 6	2.6
J1223.3+7954	8.1 ± 6.0	186 ± 502	0.1	0.3 ± 0.4	41 ± 35	-0.2
J1347.0-2956	26.1 ± 8.6	204 ± 367	0.2	2.0 ± 1.2	31 ± 17	-2.6
J1410.4+7411	40.4 ± 10.7	30 ± 18	1.2	12.4 ± 5.3	7 ± 2	-3.7
J2257.9-3646	33.9 ± 12.6	17 ± 12	1.3	9.4 ± 7.0	6 ± 3	-4.6
J2347.2+0707	36.6 ± 10.8	61 ± 49	-2.5	4.7 ± 2.6	15 ± 6	-12.1

**Table 3:** Best-fit parameters for a power law with exponential cutoff spectrum, fitting the 24-month data set between 0.1 and 300 GeV. The index was fixed to  $\Gamma = 1.5$  or  $\Gamma = 0.35$ , respectively. The table lists the normalization  $\phi_0$  and cutoff energy  $E_c$ . The column TS<sub>exp</sub> gives the likelihood ratio for the comparison with a pure power-law fit. See the text for more details on the interpretation of TS<sub>exp</sub>.

42 months	$\Gamma = 1.5$			$\Gamma = 0.35$		
2FGL name	$\phi_0/10^{-11}$ [(cm <sup>2</sup> s GeV) <sup>-1</sup> ]	$E_c$ [GeV]	TS <sub>exp</sub>	$\phi_0/10^{-11}$ [(cm <sup>2</sup> s GeV) <sup>-1</sup> ]	$E_c$ [GeV]	TS <sub>exp</sub>
J0031.0+0724	17.5 ± 7.7	38 ± 35	-6.9	1.1 ± 1.0	18 ± 11	-13.9
J0116.6-6153	27.1 ± 7.3	44 ± 30	1.2	5.8 ± 3.0	10 ± 4	-7.1
J0143.6-5844	53.6 ± 8.7	53 ± 26	3.9	13.4 ± 3.9	10 ± 2	-17.8
J0305.0-1602		$E_c \rightarrow \infty$		2.9 ± 1.7	12 ± 5	2.3
J0312.8+2013	23.4 ± 8.2	42 ± 32	0.5	3.0 ± 1.8	13 ± 5	-3.0
J0338.2+1306	32.3 ± 7.6	153 ± 177	1.1	5.8 ± 2.5	14 ± 5	-2.7
J0438.0-7331	20.5 ± 7.7	54 ± 48	0.6	2.8 ± 1.9	14 ± 6	-3.6
J0737.5-8246	29.1 ± 9.4	47 ± 38	2.2	6.4 ± 3.5	10 ± 4	2.3
J1223.3+7954	7.8 ± 4.9	103 ± 179	-0.3	0.4 ± 0.4	31 ± 23	-2.1
J1347.0-2956	27.9 ± 6.8	212 ± 285	0.3	2.1 ± 0.9	31 ± 13	-7.5
J1410.4+7411	42.0 ± 8.0	27 ± 12	4.3	15.3 ± 4.7	7 ± 1	-3.3
J2257.9-3646	19.5 ± 7.9	21 ± 15	0.8	3.3 ± 2.4	9 ± 4	-2.8
J2347.2+0707	46.9 ± 9.5	49 ± 27	-0.1	12.0 ± 4.7	8 ± 2	-14.6

**Table 4:** Best-fit parameters for a power law with exponential cutoff spectrum, fitting the 42-month data set between 0.1 and 300 GeV. The index was fixed to  $\Gamma = 1.5$  or  $\Gamma = 0.35$ , respectively. The table lists the normalization  $\phi_0$  and cutoff energy  $E_c$ . The column TS<sub>exp</sub> gives the likelihood ratio for the comparison with a pure power-law fit. See the text for more details on the interpretation of TS<sub>exp</sub>.

For the 24-month data, the upper part of table 5 lists the number of photons detected from each source between 3–10 GeV and 10–300 GeV, respectively, together with the energy and event class of the photon with highest energy. The lower part lists the same quantities



2FGL name	Number of photons ( $r \leq 0.5^\circ$ )		$N_{\text{pred}}^{\text{bg}}$ (10–300 GeV) gal/iso/ $\Sigma$	$E_{\text{max}}$ [GeV]	Evcl
	3–10 GeV	10–300 GeV			
J0031.0+0724		5	0.3/0.6/0.9	$44 \pm 4$	4
J0116.6–6153		5	0.2/0.7/0.9	$26_{-2}^{+1}$	4
J0143.6–5844	17	15	0.2/0.7/0.9	$45 \pm 3$	4
J0305.0–1602	11	6	0.3/0.6/0.9	$39_{-1}^{+2}$	4
J0312.8+2013		5	0.9/0.7/1.6	$35_{-3}^{+4}$	4
J0338.2+1306	27	8	1.3/0.6/1.9	$29 \pm 2$	4
J0438.0–7331	14	6	0.6/0.8/1.4	$56 \pm 3$	4
J0737.5–8246		7	0.9/0.6/1.5	$46_{-4}^{+5}$	4
J1223.3+7954		6	0.7/0.8/1.5	$61_{-5}^{+6}$	4
J1347.0–2956		6	0.7/0.7/1.4	$55_{-4}^{+6}$	2
J1410.4+7411	18	6	0.4/0.9/1.3	$35 \pm 2$	4
J2257.9–3646		6	0.2/0.7/0.9	$18_{-1}^{+2}$	4
J2347.2+0707	19	5	0.7/0.6/1.3	$84_{-7}^{+10}$	4

J0143.6–5844	30	23	0.5/1.3/1.8	$53 \pm 4$	4
J0305.0–1602	16	6	0.5/1.0/1.5	$39_{-1}^{+2}$	4
J0338.2+1306	38	16	2.2/1.0/3.2	$152_{-13}^{+15}$	4
J1410.4+7411	33	10	0.8/1.6/2.4	$36 \pm 2$	2

**Table 5:** *Top:* 24-month data: Number of  $\gamma$ -ray photons, listed for detected energy bins between 3–10 GeV and 10–300 GeV, within a radial region of  $0.5^\circ$  around the source’s position. Additionally, the expected numbers of background photons from Galactic foreground (gal) and isotropic background (iso) between 10–300 GeV are given. The last columns list the energy of the photon with highest energy, and its corresponding event classification assigned by LAT data reconstruction (2: SOURCE, 4: ULTRACLEAN). *Bottom:* Same as above, for 42 months of data: Number of  $\gamma$ -ray photons in the 42-month data set for spectrally preselected source candidates, see section 3.3.

for the spectrally selected list of candidates after 42 months. Additionally, the number of background photons  $N_{\text{pred}}^{\text{bg}}$  expected within  $0.5^\circ$  around the source is given for the 10–300 GeV interval. These values were derived by fitting a RoI of  $1^\circ \times 1^\circ$  centered on the position of the SoI, fixing the normalizations (and power-law correction) of the Galactic foreground and isotropic background templates to the best-fit values obtained from the entire 0.1–300 GeV fit.<sup>8</sup> On average, approximately seven photons above 10 GeV have been detected after 24 months, containing between one to two background photons within a radius of  $0.5^\circ$ . We note that only 2FGL J0338.2+1306 has been detected above 100 GeV.

The potential variability of the source flux was tested with an unbinned Kolmogorov-Smirnov (KS) test [53]. This test is already valid for a small number of photon counts, in distinction to the binned chi-square method used for the 2FGL catalog. The empirical cumulative distribution function of the arrival times of individual photons is compared to a uniform distribution, taking the (possibly varying) exposure into account. The resulting

<sup>8</sup>Owing to the quadratic-shaped RoI, the numbers were multiplied with  $\pi 0.5^2 \approx 0.785$  to correct for a circular RoI.

2FGL Name	$P_{\text{const}}$		95% upper limit $\theta_s^{95}$ [deg]	
	3–300 GeV	10–300 GeV	3–300 GeV	10–300 GeV
J0031.0+0724		0.51		0.53
J0116.6–6153		0.17		0.55
J0143.6–5844	0.97	0.83	0.25	0.38
J0305.0–1602	0.006	0.19	0.45	0.73
J0312.8+2013		0.05		0.50
J0338.2+1306	0.15	0.57	0.48	0.60
J0438.0–7331	0.28	0.33	0.30	0.50
J0737.5–8246		1.00		0.35
J1223.3+7954		0.23		0.35
J1347.0–2956		0.40		0.70
J1410.4+7411	0.78	0.66	0.38	0.60
J2257.9–3646		0.08		0.90
J2347.2+0707	0.62	0.65	0.28	0.75

J0143.6–5844	0.89	0.46	0.17	0.25
J0305.0–1602	0.004	0.04	0.45	0.70
J0338.2+1306	0.02	0.82	0.23	0.38
J1410.4+7411	0.47	0.97	0.33	0.47

**Table 6:** Probability for temporally constant  $\gamma$ -ray emission (left columns) and upper limit on the intrinsic angular extent of the signal (95% c.l., right columns). The quantities are listed for the 10–300 GeV band and, in the case of a detection between 3–10 GeV, 3–300 GeV band. Quantities derived from the 24 (42)-month data are shown in the *top* (*bottom*) panel.

probabilities  $P_{\text{const}}$  for the temporal photon distribution to be consistent with a constant flux are listed in table 6 for both the 3–300 GeV and inclusive 10–300 GeV interval. In particular, we find 2FGL J0305.0–1602 to show indications for variability ( $P_{\text{const}} = 4\%$ ).

We used a likelihood-ratio test to probe for intrinsic spatial extent. The corresponding likelihood function is given by  $L(\theta_s) = -2 \sum_{i=1}^N \ln [p_{\text{det}}(\mathbf{x}_i - \bar{\mathbf{x}}; \theta_s) + b]$ , where  $p_{\text{det}}(\mathbf{x}; \theta_s)$  follows the probability distribution function (PDF) for a photon to be detected at  $\mathbf{x}$ ,  $\bar{\mathbf{x}}$  denotes the best-fit position of the SoI, and  $b$  denotes the (flat) PDF of the underlying background  $N_{\text{pred}}^{\text{bg}}$  [10]. The PDF of  $\mathbf{x} - \bar{\mathbf{x}}$  for an intrinsically extended  $\gamma$ -ray emitter is the convolution of *Fermi*-LAT’s point spread function (PSF)  $p_{\text{PSF}}$  (version P7\_V6) with the intensity profile  $p_{\text{int}}$  of the emitter,  $p_{\text{det}} = p_{\text{PSF}} * p_{\text{int}}$ . The intensity profile  $p_{\text{int}}$  of a DM subhalo follows its line-of-sight integrated squared density profile. Similar to the approach followed in Paper I, the DM density profile of a subhalo was assumed to follow the spherically symmetric Navarro-Frenk-White (NFW) profile  $\rho(r) \propto [r/r_s (1 + r/r_s)^2]^{-1}$  [54], where  $r$  denotes the distance to the center of the halo with a characteristic value at  $r_s$ . Since 87.5% of the total luminosity are produced within  $r_s$ , it serves as a convenient proxy for the intrinsic subhalo extent. For a subhalo at distance  $D$ , this corresponds to the angle  $\theta_s \approx r_s/D$ . We remark that 68% of the total luminosity are produced within  $\theta_{68} \simeq 0.46 \theta_s$ , which is more convenient for comparison with observational data.

The minimum  $L_{\text{min}}$  of the likelihood function  $L$  arises for the extension parameter  $\theta_s$  fitting the photon distribution best. Applying the theorem of Wilks [51], the quantity

$\Delta L = L - L_{\min}$  follows a chi-square distribution with one degree of freedom, with additional terms of the order of  $1/N^{1/2}$ , which are important for a small number of counts (see also [55]).

We find no source candidate which shows indication for an intrinsic angular extent. Note that this result is in agreement with ref. [28] that also searched for angular extended sources. For each source, we present upper limits on  $\theta_s$  at 95% confidence level in table 6. For the 24-month data between 10–300 GeV, note hereby that the given confidence level is not precisely defined, owing to the low number statistics which might affect the chi-square distribution. In general, the upper limits range from  $0.2^\circ$  to  $0.9^\circ$ , where the most constraining ones can obviously be derived from the largest data sets (42 months, 3–300 GeV).

### 3.5 Multi-wavelength counterparts

#### 3.5.1 Catalog data

Although the sources in table 1 are cataloged as unassociated, we carried out a dedicated counterpart search.<sup>9</sup> In particular, radio and X-ray sources positionally located inside the 95 %-confidence-level uncertainty contour (listed in the 2FGL) of the  $\gamma$ -ray source have been searched for, providing counterpart candidates in the case of a non-DM origin. The resulting counterpart candidates are listed in table 9 (see appendix B), ordered by increasing angular separation from the 2FGL position. For every radio or X-ray source, the USNO-B1.0 catalog [56] was searched for a matching optical counterpart.

For all but one source (2FGL J1410.4+7411), at least one radio source is located nearby. However, note that owing to the high sensitivity (therefore low confusion limit) of the NVSS [57] and SUMSS [58], which were used for radio associations, the high radio source density ( $\sim 0.2 \text{ arcmin}^{-2}$ ) yields a large number of by-chance associations in the rather large positional uncertainty of the  $\gamma$ -ray sources (see table 1 and figure 2).

#### 3.5.2 WISE data

The sources 2FGL J0312.8+2013, 2FGL J0737.5–8246, and 2FGL J1347.0–2956 have recently been associated with blazar candidates selected from the WISE survey [59] on the basis of their mid-infrared (IR) colors [7]. At least one WISE object located in the positional uncertainty of these  $\gamma$ -ray sources has been found to fulfill the IR properties of ( $\gamma$ -ray) blazars, i.e., lying in the WISE gamma-ray strip. We adopted this approach [7, 60, 61] to classify IR-counterpart candidates of  $\gamma$ -ray sources by their mid-infrared color-color properties. We focus on the IR counterparts of the four spectrally selected 2FGL candidates, together with the candidate selected in Paper I, 2FGL J0031.0+0724. For each of these five 2FGL sources, an infrared counterpart candidate is listed in the WISE catalog [62], which is positionally coincident with the established radio and X-ray associations (see section 3.5.3, table 9, and section 3.6). The associations are listed in table 10 (appendix B), together with their infrared magnitudes  $W1, W2, W3$ , and  $W4$ . As described in [60, 61] and references therein, the population of blazars spans a distinct region in the infrared color space of WISE objects, the WISE Blazar Strip. In particular, the sample of known  $\gamma$ -ray emitting blazars populates the WISE gamma-ray strip (WGS), which is a subspace of the WISE Blazar Strip. The WGS can be parametrized in two (overlapping) subregions, one which is dominantly populated by  $\gamma$ -ray

<sup>9</sup>Apart from preselected catalogs, the archives NASA/IPAC Extragalactic Database (NED, <http://ned.ipac.caltech.edu/>) and HEASARC (<http://heasarc.gsfc.nasa.gov/cgi-bin/W3Browse/w3browse.pl>) were queried.

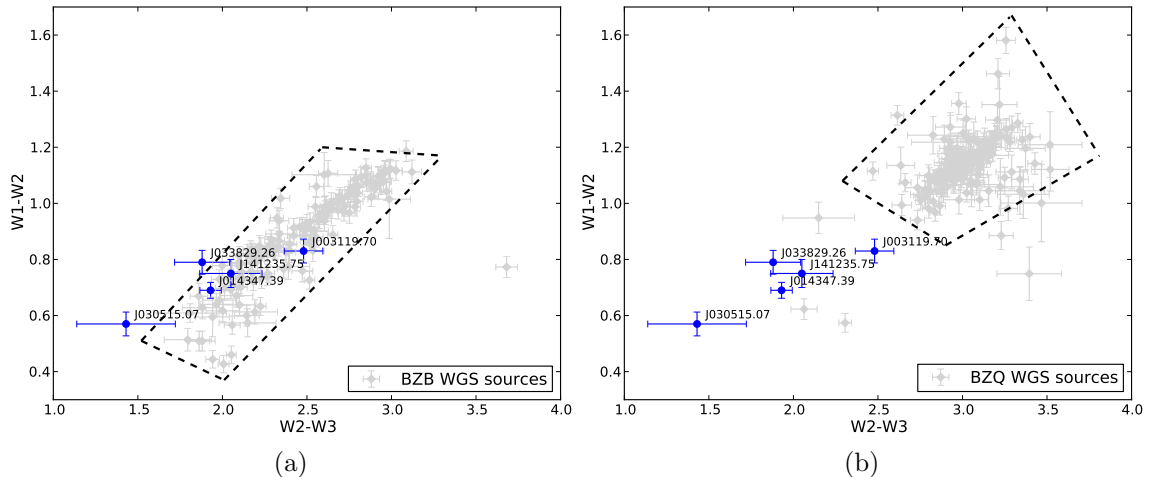


**Figure 1:** (a): Infrared color-color diagram of the WISE associations in table 10 (blue circles). The WGS subregion of BZBs is bordered with the dashed line, while the reference sources used in [61] are indicated with the gray diamonds. (b): Same as (a), comparing to the WGS subregion of BZQs.

emitting BL Lacs (BZBs), while the other one is dominated by flat spectrum radio quasars (BZQs). In figure 1, we compare the infrared color-color diagram ( $W2 - W3, W1 - W2$ ) of the WISE associations in table 10 with the BZB and BZQ regions of [61].<sup>10</sup> We find that the WISE associations for all five 2FGL sources hint at a BL Lac origin of the  $\gamma$ -ray emission, as being consistent with the BZB region of the WGS.

### 3.5.3 *Swift*-UVOT/XRT data

Besides the available catalogs of known X-ray sources, we have searched for unpublished archival observations of the remaining four objects. In a dedicated campaign [63], UV and X-ray follow-up observations of unidentified 2FGL sources have been carried out with the UVOT and X-ray telescope (XRT, 0.2–10 keV) aboard the *Swift* satellite [64, 65].

The photometric UVOT data were extracted from the products of the standard pipeline using the HEASoft 6.12 software package in combination with the calibration files (2012-04-02). The in-orbit calibration procedures are described in detail in [66]. The standard aperture of 5 arcsec was used for all filters to extract the background subtracted flux with *uvotsource*.

For the corresponding XRT data sets (see table 7 for details), calibration and screening (*xrtpipeline*) of the data acquired in photon-counting (PC) mode was done using standard screening criteria, along with the current release of calibration files (2012-04-02). Data were reduced with the HEASoft 6.11 software package. We used *Ximage* for source detection and *Xspec* (version 12.7.0) for spectral fitting. The probability limit for a background fluctuation was set to the  $5\sigma$ -level and we required a signal-to-noise ratio of  $S/N \geq 4$ . Positions and corresponding uncertainties were derived with *xrtcentroid*. For each source position, ancillary response functions needed for spectral fitting were derived with *xrtmkarf*, incorporating PSF correction. The circular on-source regions contained about 90% of the PSF (corresponding to a radius of  $\sim 47''$ ), while the background was derived from appropriate off-source regions

<sup>10</sup>Since most of the WISE sources tabulated in 10 have not been detected in the  $W4$  band, we did not attempt to use the color-color projections including  $W4$ .

FoV	Obs. ID	Obs. year	Exposure [ks]
2FGL J0143.6–5844	41274	2010	4.4
2FGL J0305.0–1602	41286	2011	3.2
2FGL J0338.2+1306	41292	2010	4.1
2FGL J1410.4+7411	47219	2012	3.5

**Table 7:** Archival *Swift*-XRT data for the celestial regions of the preselected source candidates. The columns list the observation ID, the observation year, and the total exposure in ks.

with radii between  $3'$  and  $5'$ . All X-ray sources were spectrally fit with a power-law model corrected for photoelectric absorption. The hydrogen column density  $N_{\text{H}}$  was fixed to the nominal Galactic value, calculated from the Leiden/Argentine/Bonn (LAB) HI survey [67]. For faint sources ( $S/N < 5$ ), the power-law index  $\Gamma$  was fixed to 2.0. To achieve sufficient fit quality, the spectral channels were grouped, requiring a minimum of 5 (for  $S/N < 15$ ) or 10 counts per bin, respectively. We used the Cash-statistic for spectral fitting, to properly treat the low count statistic.

In general, we find new X-ray sources in every *Swift* field of view (FoV), with (unabsorbed) fluxes between  $10^{-13}$  erg cm $^{-2}$  s $^{-1}$  and  $10^{-11}$  erg cm $^{-2}$  s $^{-1}$  in the energy band between 0.3 and 2 keV. For all selected candidates but 2FGL J1410.4+7411 some X-ray sources are positionally consistent with the cataloged  $\gamma$ -ray uncertainty, and additionally with the radio detections mentioned above (see table 9 in appendix B). Therefore, they provide convincing counterpart candidates for the  $\gamma$ -ray sources, cf. Paper I. For reference, positional and spectral parameters of every X-ray detection are listed in table 11 (appendix B).

### 3.6 Discussion of preselected candidates

Below, we provide a discussion of every preselected source candidate, based upon the results obtained in sections 3.3 to 3.5. Additionally, the updated results on 2FGL J0031.0+0724 are summarized.

Positional and spectral features of the four selected 2FGL candidates and their corresponding multi-wavelength associations (established in section 3.5) are summarized in figures 2 and 3, respectively. In figure 2, the 2FGL as well as 42-month best-fit position and their corresponding uncertainties are overlaid over the photon image measured with *Swift*-XRT, and plotted together with the positions of radio and X-ray sources. For all four 2FGL sources, the updated best-fit position shifts by a few arcmins, where the largest shift was found for 2FGL J0338.2+1306 ( $5.2'$ ). Figure 3 compares the multi-wavelength data with the average spectral energy distribution (SED) of a high-energy peaked blazar (HBL), which has been adapted from [72, 73] for particular redshifts  $z$ . Note in this context that the multi-wavelength data have not been taken contemporaneously. The redshift of each source was estimated from the distance modulus  $m_{\text{R}} - M_{\text{R}}$ , where  $m_{\text{R}}$  denotes the magnitude in the USNO-B1.0 R-band (table 9), and we assumed the detected optical emission to originate from a standard giant elliptical host galaxy with an absolute magnitude  $M_{\text{R}} = -23.1$  [74]. We assumed a vanishing K-correction, i.e., a power-law spectrum with index  $\alpha = \Gamma - 1 = 1$ . We emphasize that this method only provides a rough estimate under the given assumptions, while a precise determination of  $z$  requires spectroscopic data in the optical band. In the

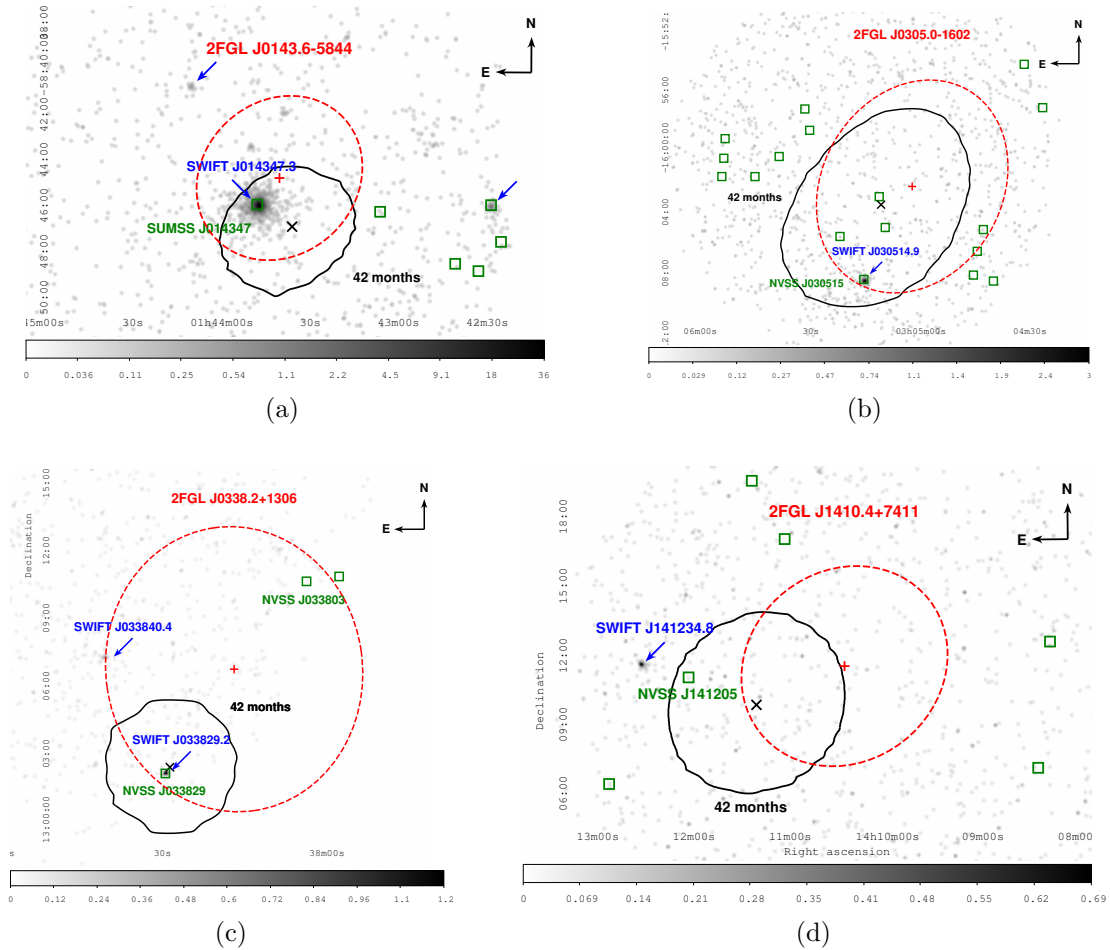


**Figure 2:** Best-fit position and uncertainty contour of (a) 2FGL J0143.6–5844, (b) 2FGL J0305.0–1602, (c) 2FGL J0338.2+1306, and (d) 2FGL J1410.4+7411 for 24 and 42 months of *Fermi*-LAT data. The cataloged position is marked with the red “+”, while the dashed red line borders its uncertainty ellipse (95% c.l.). The black “x” marks the 42-month position, and the solid black line its uncertainty contour (95% c.l.). An image of X-ray photons (*Swift*-XRT), smoothed with a Gaussian ( $7''$ ), is shown in the background. Note that the region of (c) has not been entirely observed with *Swift*-XRT, and different z-axis scales are used to improve readability (i.e., (a) log, (b) sqrt, (c) linear, and (d) linear). Positions of radio sources (NVSS) are indicated with dark-green boxes, discovered X-ray sources with blue arrows. Note that the boxes’s size does not reflect the positional uncertainty.

very high-energy regime, emitted photons are absorbed through  $\gamma$ - $\gamma$  pair production, which was calculated using the EBL model provided in [75].

**2FGL J0031.0+0724.** The 24-month *Fermi*-LAT data of this source have been intensively studied in Paper I. The analysis carried out here does not demonstrate a preference for an exponential cutoff in the 42-month data set. With a significance of  $\sim 2\sigma$ , the lightcurve of high-energy photons (10–300 GeV) is consistent with a temporally variable source, and no indication for angularly extended emission was found. In Paper I, we already claimed a possible association of the source with a faint radio source (12 mJy), positionally coincident

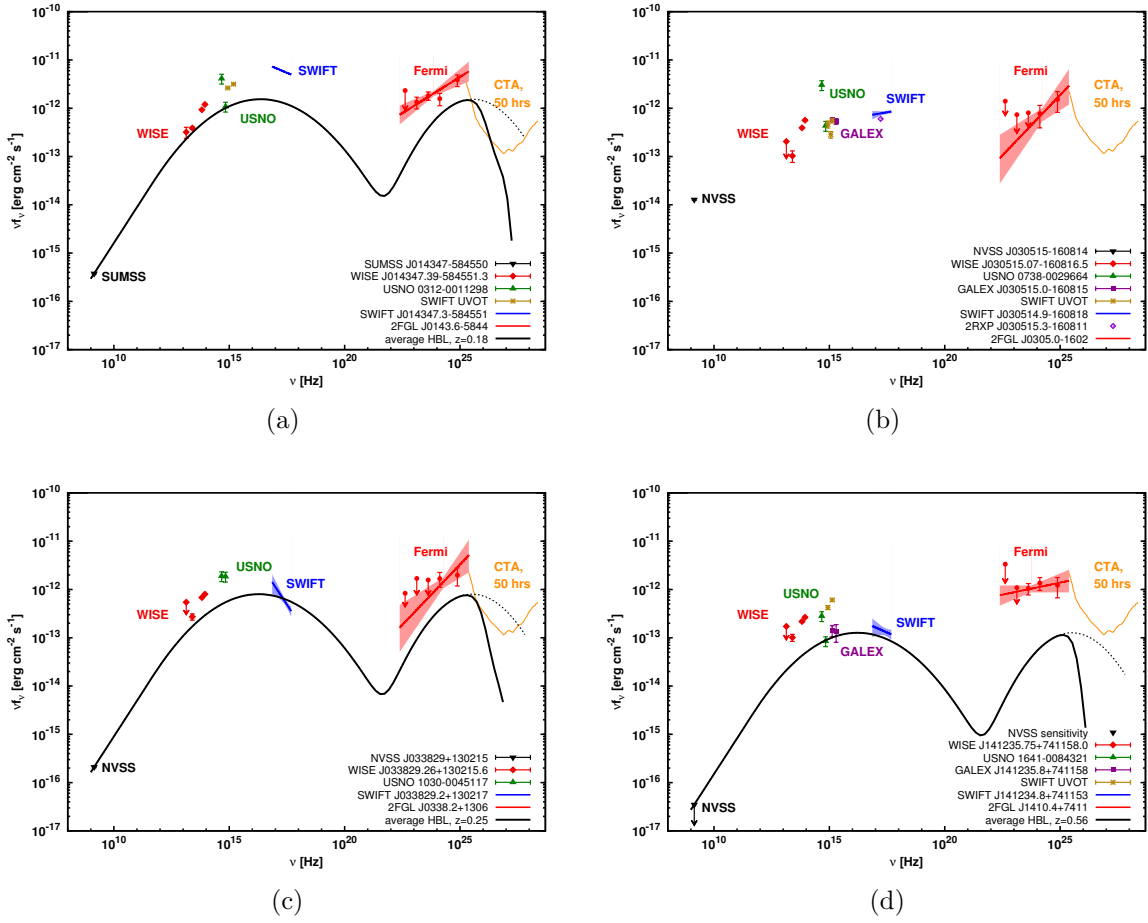


**Figure 3:** Spectral energy distribution (SED) of (a) 2FGL J0143.6–5844, (b) 2FGL J0305.0–1602, (c) 2FGL J0338.2+1306, and (d) 2FGL J1410.4+7411, assuming the multi-wavelength associations discussed in the text. Included multi-wavelength data, from low to high frequency: radio (NVSS, 1.4 GHz; black triangle), infrared (WISE,  $W4, W3, W2, W1$ ; red diamonds), optical (USNO-B1.0,  $R, B$ ; green triangles), ultra-violet (GALEX, NUV, FUV; violet boxes; see <http://galex.stsci.edu/GR6/>; *Swift*-UVOT,  $U, UVW1, UVM2, UVW2$ ; dark-golden points), X-ray (*Swift*, 0.3–2 keV; blue line),  $\gamma$ -ray (*Fermi*-LAT 2FGL, 0.1–100 GeV; red line and circles). The optical and UV data have been dereddened using  $E(B - V)$  from [68] and assuming  $R_V = 3.1$  (see [69] for details). Arrows indicate upper limits (95% c.l.). Statistical uncertainties of the X-ray and  $\gamma$ -ray spectra are indicated by the corresponding shaded areas [70]. The orange line shows the sensitivity of the planned CTA observatory for 50 hours of observation [71]. For comparison, the solid black line shows the average SED of a high-frequency peaked blazar (HBL), adapted for the estimated redshifts  $z$ . The HBL-SED is normalized to the radio flux, and the energy flux  $\nu f_\nu$  is plotted in the frame of a potential observer. The HBL-SED has been corrected for EBL absorption (see text for details), while the dotted black line shows the SED for a vanishing EBL.

with a faint X-ray source,  $f^{\text{unabs}}(0.2\text{--}2\text{ keV}) \approx 2.1 \times 10^{-13} \text{ erg cm}^{-2} \text{ s}^{-1}$ . The spectral energy distribution (SED) is consistent with a BL Lac origin (see Paper I), which is supported by the photometric infrared data of WISE J003119.70+072453.6.

**2FGL J0143.6–5844.** The 42-month data indicate the  $\gamma$ -ray spectrum to be preferentially fit with an exponential cutoff with  $\sim 3\sigma$ . Furthermore, the lightcurve is preferred to be steady, but the  $\gamma$ -ray emission is consistent with a point-source. Multi-wavelength observations show the source to be associated with a 27 mJy radio source (SUMSS), positionally coincident with the bright X-ray source SWIFT J014347.3–584551,  $f^{\text{unabs}}(0.3\text{--}2\text{ keV}) \approx 1.2 \times 10^{-11} \text{ erg cm}^{-2} \text{ s}^{-1}$ . Together with the simultaneously measured X-ray flux, the UV data seem to indicate variable emission when compared with the optical data. The infrared data support a BL Lac scenario, which is also consistent with the multi-wavelength SED, see figure 3a.

**2FGL J0305.0–1602.** While the  $\gamma$ -ray data show initial indication (at the  $2.5\sigma$  level) for a spectral cutoff at  $\sim 10\text{ GeV}$ , the temporal photon distribution of the source excludes a constant flux with  $\sim 99\%$  confidence. Multi-wavelength searches indicate the source to be positionally associated with PKS J0305–1608, showing a radio flux at the Jy level (NVSS) and an X-ray flux of  $f^{\text{unabs}}(0.3\text{--}2\text{ keV}) \approx 1.5 \times 10^{-12} \text{ erg cm}^{-2} \text{ s}^{-1}$ . The photometric infrared data are sparsely consistent with a BL Lac scenario, while the high radio flux is not in accordance with the expectation from a high-energy peaked BL Lac (see figure 3b).

**2FGL J0338.2+1306.** The source was initially selected based upon the 24-month data set, preferring a spectral cutoff with a significance of  $\sim 3\sigma$ . As shown in figure 2c, gaining photon statistics revealed a large positional shift fitting the 42-month data, and the initial indication for a spectral cutoff vanished. The updated data set also indicates a variable  $\gamma$ -ray flux at the  $2\sigma$  level. The improved positional accuracy allows us to associate 2FGL J0338.2+1306 with a radio source (15.1 mJy), which is positionally coincident with SWIFT J033829.2+130217, see figure 2c. Its WISE counterpart suggests a BL Lac origin, in accordance with the entire multi-wavelength emission (see figure 3c).

**2FGL J1410.4+7411.** The 42-month  $\gamma$ -ray data of this source prefer its spectrum to be fit with a power-law ( $\Gamma = 1.5$ ) with exponential cutoff, with a significance of  $\sim 3.3\sigma$ . The lightcurve is consistent with steady emission, but no indication for an angular extent was detected. While also being counterpartless after 24 months, the position computed from the larger photon sample seems to shift towards the faint X-ray source SWIFT J141234.8+741153, see figure 2d,  $f^{\text{unabs}}(0.3\text{--}2\text{ keV}) \approx 2.7 \times 10^{-13} \text{ erg cm}^{-2} \text{ s}^{-1}$ .<sup>11</sup> Note that the *Swift* source has no radio counterpart, which might reflect the lacking sensitivity of radio surveys. Assuming the *Swift* source to be the correct X-ray association, its infrared counterpart WISE J141235.75+741158.0 would indicate a BL Lac origin. Additionally, compared to the USNO and GALEX data, the *Swift*-UVOT observations indicate variable emission.

## 4 Discussion and conclusions

In this work, we investigated the unassociated  $\gamma$ -ray source population of the *Fermi*-LAT second year point-source catalog for sources potentially originating from DM subhalos. Basic

<sup>11</sup>Note that the X-ray source XMMSL1 J141002.6+740744 ( $f^{\text{unabs}}(0.2\text{--}2\text{ keV}) \approx 2 \times 10^{-12} \text{ erg cm}^{-2} \text{ s}^{-1}$ ) [76] is located just outside the 2FGL 95% uncertainty contour, but does not appear in the SWIFT observations.



catalog selection revealed 13 high-latitude sources, with hard  $\gamma$ -ray spectra detected above 10 GeV, and lacking indication for temporal variability. Using 3.5 years (42 months) of *Fermi*-LAT data, we developed a statistical test to probe the candidates for spectral consistency with self-annihilating DM (a power-law with exponential cutoff). The high-energy spectra of a subset of 4 sources were found to be preferentially fit by power-laws with exponential cutoff (i.e., 2FGL J0143.6–5844, 2FGL J0305.0–1602, 2FGL J0338.2+1306, and 2FGL J1410.4+7411), with significances between  $2.5\sigma$  and  $3.3\sigma$ . All sources were tested for temporally constant and spatially extended  $\gamma$ -ray emission. The  $\gamma$ -ray emission of 2FGL J0305.0–1602 shows a  $\sim 3\sigma$  indication to be temporally variable, while none of the 13 sources shows indications for angularly extended emission. Multi-wavelength studies were conducted to search for associations, using refined positional information based upon 3.5 years of *Fermi*-LAT data. For 2FGL J0143.6–5844, 2FGL J0305.0–1602, and 2FGL J0338.2+1306, we established clear associations detected in the radio, infrared, optical, UV, and X-ray bands, while 2FGL J1410.4+7411 is indicated to be associated to a faint X-ray source, which has also been detected in the infrared, optical, and UV band.

With the exception of 2FGL J0305.0–1602, the infrared color-color data of the three other sources is fully consistent with the population of BL Lacs detected with *Fermi*-LAT. In addition, such a scenario would be favored by the multi-wavelength data, in particular by the faint radio, X-ray, and hard  $\gamma$ -ray emission, indicating a scenario of a high-frequency peaked BL Lac (see figure 3 and Paper I for details). For all three cases, we note that the  $\gamma$ -ray flux predicted by the average SED is below the *Fermi*-LAT measurement. This might indicate a sample bias, meaning that the sources have been detected in a flaring state. Within the errors, the infrared association of 2FGL J0305.0–1602 might also indicate a BL Lac origin, while in particular its bright radio counterpart may point towards a different scenario. Finally, the recent study in [8] has attempted to classify the entire sample of unassociated *Fermi*-LAT sources, distinguishing between AGN-like and pulsar-like sources. Using a Random Forest (RF) classifier trained on cataloged  $\gamma$ -ray properties of associated *Fermi*-LAT sources, the major fraction of the unassociated sources are predicted to be AGN, and no significant outliers have been found. All 13 candidates we selected in table 1 are suggested to be AGN. Consistently, the recent RF classification in [9] assigns all of them to originate from BL Lacs. In particular, this strongly supports the BL Lac origin of the four spectrally selected candidates. Note, however, that since we predict  $\gamma$ -ray sources originating from DM subhalos to be particularly faint, their cataloged spectral and localization parameters suffer from large statistical uncertainties. Therefore, DM subhalos might hide in the sample of sources classified by the RF algorithm, emphasizing the necessity of the in-depth investigations carried out in this paper.

In conclusion, we find no unassociated  $\gamma$ -ray source in the 2FGL catalog which is favored to originate from a subhalo driven by self-annihilating WIMPs at a mass scale above 100 GeV. However, we conclude that, among all candidates, the source 2FGL J1410.4+7411 would be the most interesting, owing to  $\gamma$ -ray properties which might prefer a DM origin and a high uncertainty about its association. From the final source sample we can exclude 2FGL J0305.0–1602 (owing to variable  $\gamma$ -ray emission). We note that no source can be firmly excluded by spectral properties. We find the remaining candidates to most likely originate from faint BL Lacs.

Albeit our prediction of a BL Lac origin, we investigated all source candidates in the context of the recently claimed evidence for a line-like feature at  $\sim 130$  GeV in the Galactic Center region [38, 77–83]. In the case of a self-annihilating DM scenario, DM subhalos will

also appear with a  $\gamma$ -ray line at  $\sim 130$  GeV, and searches have been started in [80, 84–86]. Except for 2FGL J0338.2+1306, having a photon at 152 GeV, we note that none of the other sources has been detected above 100 GeV.

The study presented here has clearly outlined the problems of identifying faint *Fermi* sources. Difficulties are mainly related to the limiting collection area of the LAT at the high energy end, resulting in a small number of photons. This implies the consequently large uncertainty of source locations, which in turn leads to source confusion at the faint end of source populations. Likewise, the small number of photons limits the ability to determine spectral and temporal properties at the high energy end of the *Fermi*-LAT response with sufficient accuracy to distinguish source models. Finally, from the theoretical point of view in the considered DM scenario, the entirely limited number of detectable subhalos prohibits conclusive population studies.

Focussing on high-latitude sources with fluxes at the level of the studied ones, we emphasize that at least some of these issues can be addressed with larger data sets based upon longer observations. The correspondingly larger signal-to-background ratios allow us to improve the positional accuracy by a factor of  $\sim 2$  with 10 years of *Fermi*-LAT data, for instance, and to monitor the temporal photon distribution over longer time periods. The improvement in sensitivity might push the number of detectable subhalos to  $\mathcal{O}(5)$ .

In particular, the issues can also be addressed with pointed follow-up observations in the very high-energy (VHE) band. The large collection areas provided by imaging air Cherenkov telescopes (IACTs) for energies above  $\sim 50$  GeV, such as H.E.S.S.-II [87, 88], MAGIC stereo [89, 90], VERITAS [91, 92], and, in particular, the planned Cherenkov telescope array (CTA) [71, 93, 94], allow the detection of a larger photon sample, significantly reducing positional and spectral uncertainties. If detected in the VHE, source candidates therefore can be easily associated or even identified, see [27].

As a final remark, a potential successor of *Fermi*-LAT such as GAMMA-400 [95, 96] will significantly improve the observable energy range (100 MeV–3 TeV), angular resolution ( $\sim 0.01^\circ$  at 100 GeV), and energy resolution ( $\sim 1\%$  at 100 GeV). The launch of GAMMA-400 is planned for 2018. For the case of unidentified *Fermi*-LAT sources, such a telescope will constrain their celestial position with enhanced precision.

## Acknowledgments

HSZ kindly acknowledges Francesco Massaro for providing data published in [61], Jules P. Halpern, and Christoph Weniger for helpful discussions. We acknowledge the anonymous referee for useful comments. This work was supported through the collaborative research center (SFB) 676 “Particles, Strings, and the Early Universe” at the University of Hamburg. This research has made use of the NASA/IPAC Extragalactic Database (NED) which is operated by the Jet Propulsion Laboratory, California Institute of Technology, under contract with the National Aeronautics and Space Administration.

## A Probability distribution of $\text{TS}_{\text{exp}}$

To determine the probability density distribution (pdf) of  $\text{TS}_{\text{exp}}$  (eq. 3.1) in the null-hypothesis  $H_0$ , we used bootstrap Monte Carlo simulations [53]. Assuming a pure power-law spectrum (i.e.,  $H_0$ ), we simulated data of the RoI corresponding to 2FGL J0338.2+1306, which was exemplarily selected to check whether an exponential cutoff is preferred by the

actual data set (see table 3). The 25 000 simulated data sets were then analyzed with the framework described in section 3.2 and 3.3, therefore calculating  $\text{TS}_{\text{exp}}$  in exactly the same way as in the actual data analysis. Each individual analysis procedure was checked for non-converging behavior ( $\sim 14\%$ ), and the final data set of simulations was cleaned accordingly.

The simulations were done in a two-step approach: First, we used *gtobssim* to simulate five individual 24-month data sets of the RoI centered on 2FGL J0338.2+1306 (between 100 MeV and 300 GeV). All sources in the RoI were modeled with the cataloged power-law spectra, since the current version of *gtobssim* does not accept log-parabola spectra (which are sometimes preferred). Background models were implemented as described in section 3.2, and we used the actual spacecraft file of the first 24 months of data-taking. We checked the consistency between the analysis results from the simulated data and the actual data set. As a second step, the five individual simulations were merged to one data set. Applying the bootstrap technique to the merged data, we generated 25 000 individual 24-month data sets to be used in our analysis. Again, we checked that the analysis reproduced the actual data well.

Figure 4a shows the pdf of  $\text{TS}_{\text{exp}}$ , fixing the index  $\Gamma$  of the alternative hypothesis  $H_1$  (power-law with exponential cutoff) to  $\Gamma = 1.5$  and  $\Gamma = 0.35$ , respectively. The simulation shows that the pdf does indeed not follow a  $\chi^2/2$ -distribution [52] for both negative and positive  $\text{TS}_{\text{exp}}$  values. Rather, we find asymmetric pdfs with maxima and large tails at negative  $\text{TS}_{\text{exp}}$  values.<sup>12</sup> These features are more pronounced for  $\Gamma = 0.35$ , owing to the sharply peaked  $\gamma$ -ray spectrum. For the positive half-plane, the  $p$ -values  $p(> \text{TS}_{\text{exp}})$  (the significance of the test statistic) are shown in figure 4b. The  $p$ -values are compared to the prediction of Chernoff’s theorem [52], where the test statistic in the positive half-plane should follow  $0.5 [\delta(\text{TS}_{\text{exp}}) + \chi_1^2(\text{TS}_{\text{exp}})]$ , with  $\delta(x)$  the delta-function and  $\chi_1^2(x)$  the chi-square distribution with one degree of freedom. For  $\Gamma = 0.35$ , we find that for large, positive  $\text{TS}_{\text{exp}}$  the pdf approximately follows Chernoff’s theorem, while the pdf of a  $\Gamma = 1.5$  spectrum does not. The resulting significances corresponding to selected  $\text{TS}_{\text{exp}}$  values are shown in table 8. For the index  $\Gamma = 1.5$  (0.35), a significance of  $2\sigma$  corresponds to  $\text{TS}_{\text{exp}} = -6$  ( $-20$ ) and  $\text{TS}_{\text{exp}} = 2$  (2), respectively, while the  $3\sigma$  contour is given by  $\text{TS}_{\text{exp}} = -25$  ( $-35$ ) and  $\text{TS}_{\text{exp}} = 4$  (7).

---

<sup>12</sup>The maxima are at  $\text{TS}_{\text{exp}} = -0.25$  ( $-2.25$ ) for  $\Gamma = 1.5$  (0.35).

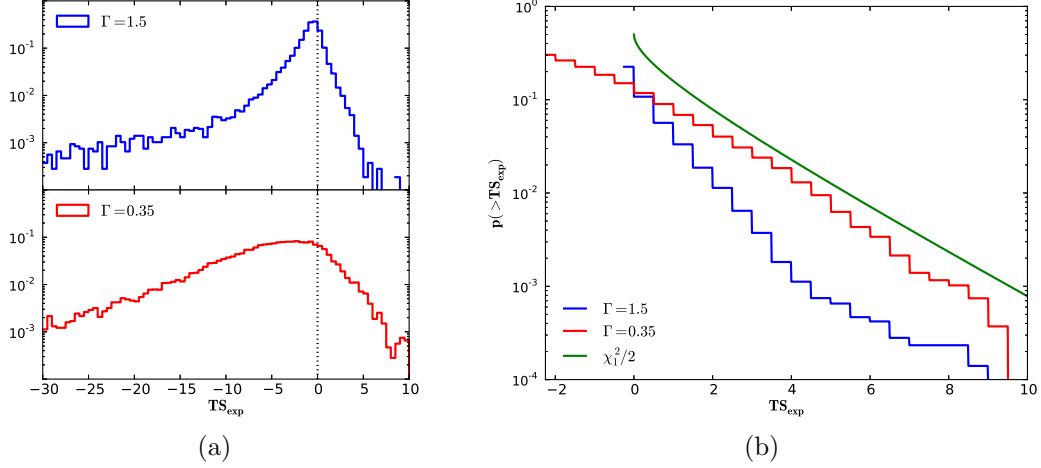


**Figure 4:** (a): Probability density distribution of the test statistic  $\text{TS}_{\text{exp}}$  in the null hypothesis  $H_0$ . The power-law index of the alternative hypothesis  $H_1$  was fixed to  $\Gamma = 1.5$  (*top*) and  $\Gamma = 0.35$  (*bottom*). The dotted vertical line indicates  $\text{TS}_{\text{exp}} = 0$ . (b): P-value  $p(> \text{TS}_{\text{exp}})$  for the positive half-plane of the distribution, starting from its corresponding maximum. The curves for  $\Gamma = 1.5$  (blue line) and  $\Gamma = 0.35$  (red line) are compared to a  $\chi_1^2/2$  distribution (green line).

$\text{TS}_{\text{exp}}$	$p(< \text{TS}_{\text{exp}}) [\sigma]$		$p(> \text{TS}_{\text{exp}}) [\sigma]$		
	$\Gamma = 1.5$	$\Gamma = 0.35$	$\text{TS}_{\text{exp}}$	$\Gamma = 1.5$	$\Gamma = 0.35$
-40.0		3.9	0.0	1.3	1.5
-35.0		3.0	2.0	2.4	2.0
-30.0	3.8	2.7	4.0	3.2	2.4
-25.0	3.0	2.4	6.0	3.5	2.9
-20.0	2.7	2.1	8.0	3.7	3.3
-15.0	2.5	1.8	10.0	4.0	4.1
-10.0	2.3	1.3			
-5.0	1.8	0.7			
0.0	0.2	0.2			

**Table 8:** Probability ( $p$ -value) to randomly find the test statistic to be lower (*left table*) or larger (*right table*) than a certain  $\text{TS}_{\text{exp}}$  value, given in Gaussian sigma. The  $p$ -value is listed for both assuming the index  $\Gamma$  of the power law with exponential cutoff to be 1.5 and 0.35, respectively.

## B Multi-wavelength association

2FGL name	Sep.	Radio	Optical (USNO-B1.0)	X-ray	WGS
J0031.0+0724	3.1'	–	0973-0005560: 19.5 <sup>m</sup> /18.2 <sup>m</sup>	SWIFT J003054.9+072328: 0.03(1)	
	3.4'	NVSS J003119+072456: 12(1) mJy	0974-0005617: 19.8 <sup>m</sup> /18.6 <sup>m</sup>	SWIFT J003119.8+072454: 0.21(7)	✓
	4.5'	–	[HB2010a] J007.70635+07.38744: 20.9 <sup>m</sup> *	SWIFT J003049.8+072316: 0.04(1)	
	6.2'	NVSS J003128+072204: 12(1) mJy	–	–	
J0116.6–6153	2.7'	SUMSS J011619–615343: 24(1) mJy/beam <sup>§</sup>	QORC J011619.6–615344, $p_{QSO} = 0.98$	–	
	3.4'	SUMSS J011656–615013: 43(2) mJy/beam <sup>§</sup>	–	–	
	3.7'	SUMSS J011643–615653: 33(1) mJy/beam <sup>§</sup>	0280-0013875: 20.0 <sup>m</sup> /15.1 <sup>m</sup>	–	
	–	–	0280-0013876: 18.0 <sup>m</sup> /15.0 <sup>m</sup>	–	
J0143.6–5844	1.6'	SUMSS J014347–584550: 27(1) mJy/beam <sup>§</sup>	0312-0011298: 18.5 <sup>m</sup> /16.6 <sup>m</sup>	SWIFT J014347.3–584551: 11.5(3) <sup>§</sup>	✓
	2.3'	NVSS J030511–160249: 7(1) mJy	–	–	
	3.2'	NVSS J030509–160450: 3(1) mJy	0739-0030568: 21.6 <sup>m</sup> /18.9 <sup>m</sup>	–	
	–	–	0739-0030569: 20.6 <sup>m</sup> /18.8 <sup>m</sup> †	–	
J0305.0–1602	5.4'	NVSS J030442–160458: 8(2) mJy	–	–	
	5.8'	NVSS J030521–160525: 47(2) mJy	–	–	
	6.9'	NVSS J030515–160814: 917(35) mJy	0738-0029664: 19.6 <sup>m</sup> /17.0 <sup>m</sup>	2RXP J030515.3–160811: 1.26	
	–	–	–	SWIFT J030514.9–160818: 1.5(1) <sup>§</sup>	
J0312.8+2013	2.4'	NVSS J031247+201606: 5.1(4) mJy	–	–	
	2.8'	NVSS J031240+201141: 18(1) mJy	1101-0034847: 21.2 <sup>m</sup> /19.4 <sup>m</sup>	–	✓ [7]
	4.7'	NVSS J031307+201229: 2.7(4) mJy	–	–	
	5.6'	NVSS J031245+201913: 4(1) mJy	1103-0035146: –/19.4 <sup>m</sup>	–	
J0338.2+1306	5.1'	NVSS J033803+131045: 28(1) mJy	–	–	
	5.5'	NVSS J033829+130215: 15.1(6) mJy	1030-0045117: 19.3 <sup>m</sup> /18.3 <sup>m</sup>	SWIFT J033829.2+130217: 1.5(4) <sup>§</sup>	✓
	3.3'	SUMSS J043836–732921: 20(1) mJy/beam <sup>§</sup>	0165-0071403: 15.6 <sup>m</sup> /14.1 <sup>m</sup>	–	
	6.3'	SUMSS J043900–732648: 63(2) mJy/beam <sup>§</sup>	0165-0071476: 17.8 <sup>m</sup> /17.0 <sup>m</sup>	–	
J0737.5–8246	2.3'	SUMSS J073706–824836: 14(1) mJy/beam <sup>§</sup>	0071-0020954: 17.8 <sup>m</sup> /17.5 <sup>m</sup>	–	✓ [7]
	1.9'	NVSS J122358+795329: 31(1) mJy	1698-0045483: 20.2 <sup>m</sup> /18.5 <sup>m</sup>	–	
	2.2'	NVSS J134706–295840: 27(1) mJy	0600-0304193: 18.8 <sup>m</sup> /17.1 <sup>m</sup>	1WGA J1347.1–2958: 0.23(4)	
	3.5'	NVSS J134653–295346: 12(1) mJy	0601-0302620: 19.8 <sup>m</sup> /18.4 <sup>m</sup>	–	✓ [7]
J1410.4+7411	4.7'	–	–	1WGA J1347.0–2952: 0.28(5)	
	–	–	–	–	✓
	0.2'	–	0532-0895676: 19.9 <sup>m</sup> /18.4 <sup>m</sup>	1WGA J2257.9–3645: 0.08(1)	
	3.7'	NVSS J225741–364833: 6.9(5) mJy	0531-0930900: 19.8 <sup>m</sup> /18.9 <sup>m</sup>	–	
J2257.9–3646	4.3'	NVSS J225815–364433: 10.6(6) mJy	0532-0895730: 19.2 <sup>m</sup> /18.1 <sup>m</sup>	1WGA J2258.2–3644: 0.21(2)	
	4.5'	NVSS J225817–364520: 7.4(5) mJy	0532-0895735: 20.7 <sup>m</sup> /18.5 <sup>m</sup>	–	
	5.2'	–	multiple	1WGA J2258.3–3647: 0.05(1)	
	7.0'	–	0533-0862976: 19.7 <sup>m</sup> /19.8 <sup>m</sup>	1WGA J2258.0–3638: 0.027(5)	
J2347.2+0707	3.9'	NVSS J234706+070351: 40(2) mJy	0970-0695942: 21.2 <sup>m</sup> /20.5 <sup>m</sup>	–	

**Table 9:** Counterpart candidates, sorted by increasing angular separation from the nominal 2FGL position. Radio and X-ray sources are located within the 95% positional uncertainty of the 2FGL source. The radio flux is given in mJy at 1.4 GHz (§: 843 MHz), while the unabsorbed X-ray flux between 0.2–2 keV (§: 0.3–2 keV) is listed in  $10^{-12}$  erg  $\text{cm}^{-2} \text{s}^{-1}$ . Apart from the *Swift* sources, the X-ray flux was derived from the cataloged count rates (2RXP [97], 1WGA [98]), assuming a power-law with index  $\Gamma = 2.0$  and a hydrogen column density  $N_H$  as obtained from the LAB survey, see section 3.5.3 (with WebPIMMS, <http://heasarc.gsfc.nasa.gov/Tools/w3pimms.html>). For every radio or X-ray source, the table lists corresponding optical counterpart candidates along with optical flux in USNO B2/R2 [†: B1/R2, \*: SDSS  $r$ ] magnitudes (HB2012a [99], QORG [100]). Parentheses indicate the error on the last decimal. The last column indicates sources associated with infrared (WISE) blazar candidates, see section 3.5.2 in this paper and [7].

2FGL name	WISE name	W1 [mag]	W2 [mag]	W3 [mag]	W4 [mag]
J0031.0+0724	J003119.70+072453.6	13.89(3)	13.06(3)	10.58(11)	8.47(39)
J0143.6-5844	J014347.39-584551.3	13.39(2)	12.70(2)	10.77(6)	8.88(28)
J0305.0-1602	J030515.07-160816.5	14.21(3)	13.64(3)	12.21(29)	9.36
J0338.2+1306	J033829.26+130215.6	13.83(3)	13.04(3)	11.16(16)	8.30
J1410.4+7411	J141235.75+741158.0	15.03(3)	14.28(4)	12.23(18)	9.55

**Table 10:** Infrared sources detected with WISE [62], positionally coinciding with the radio and X-ray associations established for the preselected 2FGL candidate sample. We list the WISE magnitudes  $W1$ ,  $W2$ ,  $W3$ , and  $W4$ , corresponding to the 3.4, 4.6, 12, and 22  $\mu\text{m}$  bands. The error on the last decimals is written in parentheses. If no error is given, the value represents an upper limit (95 % confidence level).

Obs. ID	Name SWIFT	$\sigma_{90}$ [arcsec]	$S/N$	$N_{\text{H}}$ [ $10^{20} \text{ cm}^{-2}$ ]	$f^{\text{abs}}(0.3-2 \text{ keV})$ [ $10^{-13} \text{ erg cm}^{-2} \text{ s}^{-1}$ ]	$\phi_0$ [ $10^{-4} \text{ keV}^{-1} \text{ cm}^{-2} \text{ s}^{-1}$ ]	$\Gamma$	$C_{\text{stat}}/\text{dof}$	$f^{\text{unabs}}(0.3-2 \text{ keV})$ [ $10^{-13} \text{ erg cm}^{-2} \text{ s}^{-1}$ ]
41274	J014229.0-584553	5	7.4	2.13	$3.03^{+0.30}_{-0.48}$	$1.21^{+0.20}_{-0.18}$	$1.56^{+0.23}_{-0.22}$	9.9/10	$3.37^{+0.61}_{-0.56}$
	J014347.3-584551	4	47.4	2.04	$100.02^{+0.58}_{-0.53}$	$35.76^{+0.80}_{-0.80}$	$2.20^{+0.03}_{-0.03}$	125.3/145	$115.10^{+3.06}_{-3.03}$
41286	J014410.1-584042	6	4.1	2.03	$0.86^{+0.22}_{-0.22}$	$0.32^{+0.08}_{-0.08}$	2.00	2.2/3	$0.97^{+0.24}_{-0.24}$
41292	J030514.9-160818	4	13.1	3.62	$12.18^{+1.14}_{-1.06}$	$5.03^{+0.42}_{-0.40}$	$1.92^{+0.12}_{-0.12}$	26.9/30	$14.98^{+1.48}_{-1.43}$
	J033829.2+130217	5	6.5	15.30	$5.65^{+1.02}_{-0.87}$	$3.68^{+0.59}_{-0.54}$	$2.73^{+0.31}_{-0.32}$	6.1/7	$14.58^{+3.51}_{-3.39}$
	J033840.4+130722	5	4.4	15.20	$1.00^{+0.22}_{-0.21}$	$0.65^{+0.15}_{-0.13}$	2.00	3.2/4	$1.99^{+0.40}_{-0.40}$
47219	J141234.8+741153	5	5.4	2.35	$2.33^{+0.35}_{-0.46}$	$0.85^{+0.16}_{-0.15}$	$2.21^{+0.29}_{-0.28}$	11.1/5	$2.74^{+0.63}_{-0.58}$

**Table 11:** List of X-ray sources detected with *Swift*-XRT, sorted by right ascension. Apart from positional information (SWIFT JHHMMSS.s $\pm$ DDMMSS, where  $\sigma_{90}$  denotes the uncertainty at 90% confidence), the table lists the signal-to-noise ratio of the absorbed flux  $f^{\text{abs}}$  between 0.3 and 2 keV for each observation (Obs.ID). The spectra were fit with a power-law model corrected for photoelectric absorption (normalization  $\phi_0$ , power-law index  $\Gamma$ ), fixing the hydrogen column density  $N_{\text{H}}$  to the nominal Galactic value. The C-statistic as implemented in *Xspec* was used for spectral fitting ( $C_{\text{stat}}$ , dof denotes the number of degrees of freedom). The unabsorbed flux  $f^{\text{unabs}}$  between 0.3 and 2 keV was derived from the power-law fit.

## References

- [1] W. B. Atwood, A. A. Abdo, M. Ackermann, et al., *The Large Area Telescope on the Fermi Gamma-Ray Space Telescope Mission*, *ApJ* **697** (2009) 1071–1102, [[arXiv:0902.1089](#)].
- [2] P. L. Nolan, A. A. Abdo, M. Ackermann, et al., *Fermi Large Area Telescope Second Source Catalog*, *ApJS* **199** (2012) 31, [[arXiv:1108.1435](#)].
- [3] M. Ackermann, M. Ajello, A. Allafort, et al., *The Second Catalog of Active Galactic Nuclei Detected by the Fermi Large Area Telescope*, *ApJ* **743** (2011) 171, [[arXiv:1108.1420](#)].
- [4] N. Mirabal, D. Nieto, and S. Pardo, *The exotic fraction among unassociated Fermi sources*, [arXiv:1007.2644](#).
- [5] J. B. Stephen, L. Bassani, R. Landi, et al., *Using the ROSAT catalogue to find counterparts for unidentified objects in the first Fermi/LAT catalogue*, *MNRAS* **408** (2010) 422–429, [[arXiv:1004.5232](#)].
- [6] M. Ackermann, M. Ajello, A. Allafort, et al., *A Statistical Approach to Recognizing Source Classes for Unassociated Sources in the First Fermi-LAT Catalog*, *ApJ* **753** (2012) 83, [[arXiv:1108.1202](#)].
- [7] F. Massaro, R. D’Abrusco, G. Tosti, M. Ajello, A. Paggi, and D. Gasparrini, *Unidentified  $\gamma$ -Ray Sources: Hunting  $\gamma$ -Ray Blazars*, *ApJ* **752** (2012) 61, [[arXiv:1203.3801](#)].
- [8] N. Mirabal, V. Frias-Martinez, T. Hassan, and E. Frias-Martinez, *Fermi’s Sibyl: Mining the gamma-ray sky for dark matter subhaloes*, [arXiv:1205.4825](#).
- [9] T. Hassan, N. Mirabal, J. L. Contreras, and I. Oya, *Gamma-Ray Active Galactic Nucleus Type through Machine-Learning Algorithms*, *ArXiv e-prints* (2012) [[arXiv:1209.4359](#)].
- [10] H.-S. Zechlin, M. V. Fernandes, D. Elsässer, and D. Horns, *Dark matter subhaloes as gamma-ray sources and candidates in the first Fermi-LAT catalogue*, *A&A* **538** (2012) A93, [[arXiv:1111.3514](#)].
- [11] A. A. Abdo, M. Ackermann, M. Ajello, et al., *Spectrum of the Isotropic Diffuse Gamma-Ray Emission Derived from First-Year Fermi Large Area Telescope Data*, *Physical Review Letters* **104** (2010), no. 10 101101, [[arXiv:1002.3603](#)].
- [12] A. A. Abdo, M. Ackermann, M. Ajello, et al., *The Fermi-LAT High-Latitude Survey: Source Count Distributions and the Origin of the Extragalactic Diffuse Background*, *ApJ* **720** (2010) 435–453, [[arXiv:1003.0895](#)].
- [13] A. Cuoco, E. Komatsu, and J. Siegal-Gaskins, *Joint anisotropy and source count constraints on the contribution of blazars to the diffuse gamma-ray background*, [arXiv:1202.5309](#).
- [14] G. Jungman, M. Kamionkowski, and K. Griest, *Supersymmetric dark matter*, *Phys. Rep.* **267** (1996) 195–373, [[hep-ph/9506380](#)].
- [15] G. Bertone, D. Hooper, and J. Silk, *Particle dark matter: evidence, candidates and constraints*, *Phys. Rep.* **405** (2005) 279–390, [[hep-ph/0404175](#)].
- [16] G. Bertone, *The moment of truth for WIMP dark matter*, *Nature* **468** (2010) 389–393, [[arXiv:1011.3532](#)].
- [17] J. Diemand, M. Kuhlen, P. Madau, et al., *Clumps and streams in the local dark matter distribution*, *Nature* **454** (2008) 735–738, [[arXiv:0805.1244](#)].
- [18] V. Springel, S. D. M. White, C. S. Frenk, et al., *Prospects for detecting supersymmetric dark matter in the Galactic halo*, *Nature* **456** (2008) 73–76, [[arXiv:0809.0894](#)].
- [19] E. Komatsu, K. M. Smith, J. Dunkley, et al., *Seven-year Wilkinson Microwave Anisotropy Probe (WMAP) Observations: Cosmological Interpretation*, *ApJS* **192** (2011) 18, [[arXiv:1001.4538](#)].

- [20] S. P. Martin, *A Supersymmetry Primer*, in *Perspectives on Supersymmetry* (G. L. Kane, ed.), p. 1, 1998. [hep-ph/9709356](#).
- [21] ATLAS Collaboration, *Search for supersymmetry in events with three leptons and missing transverse momentum in  $\sqrt{s} = 7$  TeV pp collisions with the ATLAS detector*, [arXiv:1204.5638](#).
- [22] CMS Collaboration, *Search for anomalous production of multilepton events in pp collisions at  $\sqrt{s}=7$  TeV*, [arXiv:1204.5341](#).
- [23] T. Saab, *An Introduction to Dark Matter Direct Detection Searches & Techniques*, 2012. [arXiv:1203.2566](#).
- [24] M. Cirelli, G. Corcella, A. Hektor, G. Hütsi, M. Kadastik, P. Panci, M. Raidal, F. Sala, and A. Strumia, *PPPC 4 DM ID: a poor particle physicist cookbook for dark matter indirect detection*, *J. Cosmology Astropart. Phys.* **3** (2011) 51, [\[arXiv:1012.4515\]](#).
- [25] M. R. Buckley and D. Hooper, *Dark matter subhalos in the Fermi first source catalog*, *Phys. Rev. D* **82** (2010), no. 6 063501, [\[arXiv:1004.1644\]](#).
- [26] P. Brun, E. Moulin, J. Diemand, and J.-F. Glicenstein, *Searches for dark matter subhaloes with wide-field Cherenkov telescope surveys*, *Phys. Rev. D* **83** (2011), no. 1 015003, [\[arXiv:1012.4766\]](#).
- [27] **MAGIC** Collaboration, D. Nieto, J. Aleksić, J. A. Barrio, et al., *The search for galactic dark matter clump candidates with Fermi and MAGIC*, Proceedings of the 32nd International Cosmic Ray Conference (ICRC), Beijing, China, 2011. [arXiv:1109.5935](#).
- [28] M. Ackermann, A. Albert, L. Baldini, et al., *Search for Dark Matter Satellites Using Fermi-LAT*, *ApJ* **747** (2012) 121, [\[arXiv:1201.2691\]](#).
- [29] A. V. Belikov, M. R. Buckley, and D. Hooper, *Searching for dark matter subhalos in the Fermi-LAT second source catalog*, *Phys. Rev. D* **86** (2012), no. 4 043504, [\[arXiv:1111.2613\]](#).
- [30] T. Bringmann, *Particle models and the small-scale structure of dark matter*, *New Journal of Physics* **11** (2009), no. 10 105027, [\[arXiv:0903.0189\]](#).
- [31] M. Boylan-Kolchin, J. S. Bullock, and M. Kaplinghat, *Too big to fail? The puzzling darkness of massive Milky Way subhaloes*, *MNRAS* **415** (2011) L40–L44, [\[arXiv:1103.0007\]](#).
- [32] T. M. Brown, J. Tumlinson, M. Geha, et al., *The Primeval Populations of the Ultra-faint Dwarf Galaxies*, *ApJ* **753** (2012) L21, [\[arXiv:1206.0941\]](#).
- [33] M. Kuhlen, J. Diemand, and P. Madau, *The Dark Matter Annihilation Signal from Galactic Substructure: Predictions for GLAST*, *ApJ* **686** (2008) 262–278, [\[arXiv:0805.4416\]](#).
- [34] G. D. Martinez, J. S. Bullock, M. Kaplinghat, L. E. Strigari, and R. Trotta, *Indirect Dark Matter detection from Dwarf satellites: joint expectations from astrophysics and supersymmetry*, *J. Cosmology Astropart. Phys.* **6** (2009) 14, [\[arXiv:0902.4715\]](#).
- [35] L. Bergström, T. Bringmann, M. Eriksson, and M. Gustafsson, *Gamma Rays from Kaluza-Klein Dark Matter*, *Physical Review Letters* **94** (2005), no. 13 131301, [\[astro-ph/0410359\]](#).
- [36] L. Bergström, T. Bringmann, M. Eriksson, and M. Gustafsson, *Gamma Rays from Heavy Neutralino Dark Matter*, *Physical Review Letters* **95** (2005), no. 24 241301, [\[hep-ph/0507229\]](#).
- [37] T. Bringmann, L. Bergström, and J. Edsjö, *New gamma-ray contributions to supersymmetric dark matter annihilation*, *Journal of High Energy Physics* **1** (2008) 49, [\[arXiv:0710.3169\]](#).
- [38] T. Bringmann, X. Huang, A. Ibarra, S. Vogl, and C. Weniger, *Fermi LAT search for internal bremsstrahlung signatures from dark matter annihilation*, *J. Cosmology Astropart. Phys.* **7** (2012) 54, [\[arXiv:1203.1312\]](#).



- [39] N. Arkani-Hamed, D. P. Finkbeiner, T. R. Slatyer, and N. Weiner, *A theory of dark matter*, Phys. Rev. D **79** (2009), no. 1 015014–+.
- [40] M. Kuhlen, P. Madau, and J. Silk, *Exploring Dark Matter with Milky Way Substructure*, *Science* **325** (2009) 970–, [[arXiv:0907.0005](#)].
- [41] E. A. Baltz and L. Wai, *Diffuse inverse Compton and synchrotron emission from dark matter annihilations in galactic satellites*, Phys. Rev. D **70** (2004), no. 2 023512, [[astro-ph/0403528](#)].
- [42] S. Colafrancesco, S. Profumo, and P. Ullio, *Detecting dark matter WIMPs in the Draco dwarf: A multiwavelength perspective*, Phys. Rev. D **75** (2007), no. 2 023513, [[astro-ph/0607073](#)].
- [43] T. E. Jeltema and S. Profumo, *Searching for Dark Matter with X-Ray Observations of Local Dwarf Galaxies*, ApJ **686** (2008) 1045–1055, [[arXiv:0805.1054](#)].
- [44] E. A. Baltz, J. E. Taylor, and L. L. Wai, *Can Astrophysical Gamma-Ray Sources Mimic Dark Matter Annihilation in Galactic Satellites?*, ApJ **659** (2007) L125–L128, [[astro-ph/0610731](#)].
- [45] A. A. Abdo, M. Ackermann, M. Ajello, et al., *The First Fermi Large Area Telescope Catalog of Gamma-ray Pulsars*, ApJS **187** (2010) 460–494, [[arXiv:0910.1608](#)].
- [46] M. Kerr, F. Camilo, T. J. Johnson, et al., *Five New Millisecond Pulsars from a Radio Survey of 14 Unidentified Fermi-LAT Gamma-Ray Sources*, ApJ **748** (2012) L2, [[arXiv:1201.5160](#)].
- [47] P. S. Ray, A. A. Abdo, D. Parent, et al., *Radio Searches of Fermi LAT Sources and Blind Search Pulsars: The Fermi Pulsar Search Consortium*, 2011 Fermi Symposium proceedings - eConf C110509, Rome, Italy, 2012. [arXiv:1205.3089](#).
- [48] N. Fornengo, L. Pieri, and S. Scopel, *Neutralino annihilation into  $\gamma$  rays in the Milky Way and in external galaxies*, Phys. Rev. D **70** (2004), no. 10 103529, [[hep-ph/0407342](#)].
- [49] J. A. R. Cembranos, A. de La Cruz-Dombriz, A. Dobado, R. A. Lineros, and A. L. Maroto, *Photon spectra from WIMP annihilation*, Phys. Rev. D **83** (2011), no. 8 083507, [[arXiv:1009.4936](#)].
- [50] L. Bergström, P. Ullio, and J. H. Buckley, *Observability of gamma rays from dark matter neutralino annihilations in the Milky Way halo*, *Astroparticle Physics* **9** (1998) 137–162, [[astro-ph/9712318](#)].
- [51] S. S. Wilks, *The Large-Sample Distribution of the Likelihood Ratio for Testing Composite Hypotheses*, *Ann. Math. Statist.* **9** (1938), no. 1 60–62.
- [52] H. Chernoff, *On the Distribution of the Likelihood Ratio*, *Ann. Math. Statist.* **25** (1954), no. 3 573–578.
- [53] W. H. Press, S. A. Teukolsky, W. T. Vetterling, and B. P. Flannery, *Numerical Recipes: The Art of Scientific Computing*. Cambridge University Press, Third ed., 2007.
- [54] J. F. Navarro, C. S. Frenk, and S. D. M. White, *A Universal Density Profile from Hierarchical Clustering*, ApJ **490** (1997) 493, [[astro-ph/9611107](#)].
- [55] W. Cash, *Parameter estimation in astronomy through application of the likelihood ratio*, ApJ **228** (1979) 939–947.
- [56] D. G. Monet, S. E. Levine, B. Canzian, et al., *The USNO-B Catalog*, AJ **125** (2003) 984–993, [[astro-ph/0210694](#)].
- [57] J. J. Condon, W. D. Cotton, E. W. Greisen, et al., *The NRAO VLA Sky Survey*, AJ **115** (1998) 1693–1716.
- [58] T. Mauch, T. Murphy, H. J. Buttery, et al., *SUMSS: a wide-field radio imaging survey of the southern sky - II. The source catalogue*, MNRAS **342** (2003) 1117–1130, [[astro-ph/0303188](#)].

- [59] E. L. Wright, P. R. M. Eisenhardt, A. K. Mainzer, et al., *The Wide-field Infrared Survey Explorer (WISE): Mission Description and Initial On-orbit Performance*, *AJ* **140** (2010) 1868–1881, [[arXiv:1008.0031](#)].
- [60] R. D’Abrusco, F. Massaro, M. Ajello, J. E. Grindlay, H. A. Smith, and G. Tosti, *Infrared Colors of the Gamma-Ray-detected Blazars*, *ApJ* **748** (2012) 68, [[arXiv:1203.0568](#)].
- [61] F. Massaro, R. D’Abrusco, G. Tosti, M. Ajello, D. Gasparrini, J. E. Grindlay, and H. A. Smith, *The WISE Gamma-Ray Strip Parameterization: The Nature of the Gamma-Ray Active Galactic Nuclei of Uncertain Type*, *ApJ* **750** (2012) 138, [[arXiv:1203.1330](#)].
- [62] R. M. Cutri and et al., *WISE All-Sky Data Release (Cutri+ 2012)*, *VizieR Online Data Catalog* **2311** (2012).
- [63] A. Falcone, M. Stroh, E. Ferrara, et al., *Systematic Search for X-ray Counterparts of Fermi-LAT Unassociated Sources Using Swift Observations*, vol. 12 of *AAS/High Energy Astrophysics Division*, p. 04.03, 2011.
- [64] N. Gehrels, G. Chincarini, P. Giommi, et al., *The Swift Gamma-Ray Burst Mission*, *ApJ* **611** (2004) 1005–1020.
- [65] N. Gehrels, G. Chincarini, P. Giommi, et al., *Erratum: “The Swift Gamma-Ray Burst Mission” (ApJ, 611, 1005 [2004])*, *ApJ* **621** (2005) 558–558.
- [66] T. S. Poole, A. A. Breeveld, M. J. Page, et al., *Photometric calibration of the Swift ultraviolet/optical telescope*, *MNRAS* **383** (2008) 627–645, [[arXiv:0708.2259](#)].
- [67] P. M. W. Kalberla, W. B. Burton, D. Hartmann, et al., *The Leiden/Argentine/Bonn (LAB) Survey of Galactic HI. Final data release of the combined LDS and IAR surveys with improved stray-radiation corrections*, *A&A* **440** (2005) 775–782, [[astro-ph/0504140](#)].
- [68] D. J. Schlegel, D. P. Finkbeiner, and M. Davis, *Maps of Dust Infrared Emission for Use in Estimation of Reddening and Cosmic Microwave Background Radiation Foregrounds*, *ApJ* **500** (1998) 525, [[astro-ph/9710327](#)].
- [69] J. A. Cardelli, G. C. Clayton, and J. S. Mathis, *The relationship between infrared, optical, and ultraviolet extinction*, *ApJ* **345** (1989) 245–256.
- [70] A. A. Abdo, M. Ackermann, M. Ajello, et al., *Fermi Observations of TeV-Selected Active Galactic Nuclei*, *ApJ* **707** (2009) 1310–1333, [[arXiv:0910.4881](#)].
- [71] The CTA Consortium, *Design Concepts for the Cherenkov Telescope Array*, [[arXiv:1008.3703](#)].
- [72] G. Fossati, A. Celotti, G. Ghisellini, and L. Maraschi, *Unifying models for X-ray-selected and radio-selected BL Lac objects*, *MNRAS* **289** (1997) 136–150, [[astro-ph/9704113](#)].
- [73] D. Donato, G. Ghisellini, G. Tagliaferri, and G. Fossati, *Hard X-ray properties of blazars*, *A&A* **375** (2001) 739–751, [[astro-ph/0105203](#)].
- [74] K. Nilsson, M. Pasanen, L. O. Takalo, E. Lindfors, A. Berdyugin, S. Ciprini, and J. Pforr, *Host galaxy subtraction of TeV candidate BL Lacertae objects*, *A&A* **475** (2007) 199–207, [[arXiv:0709.2533](#)].
- [75] A. Franceschini, G. Rodighiero, and M. Vaccari, *Extragalactic optical-infrared background radiation, its time evolution and the cosmic photon-photon opacity*, *A&A* **487** (2008) 837–852, [[arXiv:0805.1841](#)].
- [76] R. D. Saxton, A. M. Read, P. Esquej, et al., *The first XMM-Newton slew survey catalogue: XMMSL1*, *A&A* **480** (2008) 611–622, [[arXiv:0801.3732](#)].
- [77] C. Weniger, *A tentative gamma-ray line from Dark Matter annihilation at the Fermi Large Area Telescope*, *J. Cosmology Astropart. Phys.* **8** (2012) 7, [[arXiv:1204.2797](#)].

- [78] M. Su and D. P. Finkbeiner, *Strong Evidence for Gamma-ray Line Emission from the Inner Galaxy*, *ArXiv e-prints* (2012) [[arXiv:1206.1616](#)].
- [79] D. P. Finkbeiner, M. Su, and C. Weniger, *Is the 130 GeV Line Real? A Search for Systematics in the Fermi-LAT Data*, *ArXiv e-prints* (2012) [[arXiv:1209.4562](#)].
- [80] A. Hektor, M. Raidal, and E. Tempel, *Fermi-LAT gamma-ray signal from Earth Limb, systematic detector effects and their implications for the 130 GeV gamma-ray excess*, *ArXiv e-prints* (2012) [[arXiv:1209.4548](#)].
- [81] L. Bergström, G. Bertone, J. Conrad, C. Farnier, and C. Weniger, *Investigating Gamma-Ray Lines from Dark Matter with Future Observatories*, *ArXiv e-prints* (2012) [[arXiv:1207.6773](#)].
- [82] E. Tempel, A. Hektor, and M. Raidal, *Fermi 130 GeV gamma-ray excess and dark matter annihilation in sub-haloes and in the Galactic centre*, *J. Cosmology Astropart. Phys.* **9** (2012) 32, [[arXiv:1205.1045](#)].
- [83] A. Hektor, M. Raidal, and E. Tempel, *An evidence for indirect detection of dark matter from galaxy clusters in Fermi-LAT data*, *ArXiv e-prints* (2012) [[arXiv:1207.4466](#)].
- [84] M. Su and D. P. Finkbeiner, *Double Gamma-ray Lines from Unassociated Fermi-LAT Sources*, *ArXiv e-prints* (2012) [[arXiv:1207.7060](#)].
- [85] D. Hooper and T. Linden, *Are Lines From Unassociated Gamma-Ray Sources Evidence For Dark Matter Annihilation?*, *ArXiv e-prints* (2012) [[arXiv:1208.0828](#)].
- [86] N. Mirabal, *The Dark Knight Falters*, *ArXiv e-prints* (2012) [[arXiv:1208.1693](#)].
- [87] P. Vincent, *H.E.S.S. Phase II*, in *International Cosmic Ray Conference*, vol. 5, pp. 163–+, 2005.
- [88] F. Aharonian, A. G. Akhperjanian, A. R. Bazer-Bachi, et al., *Observations of the Crab nebula with HESS*, *A&A* **457** (2006) 899–915, [[astro-ph/0607333](#)].
- [89] J. Albert, E. Aliu, H. Anderhub, et al., *VHE  $\gamma$ -Ray Observation of the Crab Nebula and its Pulsar with the MAGIC Telescope*, *ApJ* **674** (2008) 1037–1055, [[arXiv:0705.3244](#)].
- [90] D. B. Tridon, T. Schweizer, F. Goebel, R. Mirzoyan, and M. Teshima, *The MAGIC-II gamma-ray stereoscopic telescope system*, *Nuclear Instruments and Methods in Physics Research A* **623** (2010) 437–439. for the MAGIC Collaboration.
- [91] T. C. Weekes, H. Badran, S. D. Biller, et al., *VERITAS: the Very Energetic Radiation Imaging Telescope Array System*, *Astroparticle Physics* **17** (2002) 221–243, [[astro-ph/0108478](#)].
- [92] J. Holder, E. Aliu, T. Arlen, et al., *VERITAS: Status and Highlights*, Proceedings of the 32nd International Cosmic Ray Conference (ICRC), Beijing, China, 2011. [[arXiv:1111.1225](#)].
- [93] **CTA** Collaboration, M. Doro, *CTA—A project for a new generation of Cherenkov telescopes*, *Nuclear Instruments and Methods in Physics Research A* **630** (2011) 285–290.
- [94] M. Doro, J. Conrad, D. Emmanoulopoulos, et al., *Dark Matter and Fundamental Physics with the Cherenkov Telescope Array*, [[arXiv:1208.5356](#)]. for the CTA Collaboration.
- [95] A. M. Galper, O. Adriani, R. L. Aptekar, et al., *Status of the GAMMA-400 Project*, *ArXiv e-prints* (2012) [[arXiv:1201.2490](#)].
- [96] A. M. Galper, O. Adriani, R. L. Aptekar, et al., *Design and Performance of the GAMMA-400 Gamma-Ray Telescope for the Dark Matter Searches*, *ArXiv e-prints* (2012) [[arXiv:1210.1457](#)].
- [97] ROSAT Consortium, *ROSAT News No. 74*, *ROSAT News* (2001).
- [98] N. E. White, P. Giommi, and L. Angelini, *The WGACAT version of ROSAT sources (White+ 2000)*, *VizieR Online Data Catalog* **9031** (2000) 0.

- [99] J. B. Hutchings and L. Bianchi, *A Catalog of 19,100 Quasi-stellar Object Candidates with Redshift 0.5-1.5*, *AJ* **140** (2010) 1987–1994.
- [100] E. Flesch and M. J. Hardcastle, *An all-sky optical catalogue of radio/X-ray sources*, *A&A* **427** (2004) 387–392, [[astro-ph/0407310](#)].